AIChE

Dynamic Optimization of the Methylmethacrylate Cell-Cast Process for Plastic Sheet Production

Martín Rivera-Toledo
Departamento de Ingeniería y Ciencias Químicas, Universidad Iberoamericana Prolongación Paseo de la Reforma 880, México D.F., 01219, México

Facultad de Química, Departamento de Ingeniería Química, Universidad Nacional Autónoma de México (UNAM), México D.F., 04510, México

Antonio Flores-Tlacuahuac
Departamento de Ingeniería y Ciencias Químicas, Universidad Iberoamericana Prolongación Paseo de la Reforma 880, México D.F., 01219, México

Leopoldo Vílchis-Ramírez
Consejo Nacional de Ciencia y Tecnología (CONACyT), Av. Insurgentes Sur 1582, México D.F., 03940, México

DOI 10.1002/aic.11841
Published online April 28, 2009 in Wiley InterScience (www.interscience.wiley.com).

Traditionally, the methylmethacrylate (MMA) polymerization reaction process for plastic sheet production has been carried out using warming baths. However, it has been observed that the manufactured polymer tends to feature poor homogeneity characteristics measured in terms of properties like molecular weight distribution. Nonhomogeneous polymer properties should be avoided because they give rise to a product with undesired wide quality characteristics. To improve homogeneity properties force-circulated warm air reactors have been proposed, such reactors are normally operated under isothermal air temperature conditions. However, we demonstrate that dynamic optimal warming temperature profiles lead to a polymer sheet with better homogeneity characteristics, especially when compared against simple isothermal operating policies. In this work, the dynamic optimization of a heating and polymerization reaction process for plastic sheet production in a force-circulated warm air reactor is addressed. The optimization formulation is based on the dynamic representation of the two-directional heating and reaction process taking place within the system, and includes kinetic equations for the bulk free radical polymerization reactions of MMA. The mathematical model is cast as a time dependent partial differential equation (PDE) system, the optimal heating profile calculation turns out to be a dynamic optimization problem embedded in a distributed parameter system. A simultaneous optimization approach is selected to solve the dynamic optimization problem. Trough full discretization of all decision variables, a nonlinear programming (NLP) model is obtained and solved by using the IPOPT optimization solver. The results are presented about the dynamic optimization for two plastic sheets of different thickness and compared them against simple operating policies. © 2009 American Institute of Chemical Engineers *AIChE J,* 55: 1464–1486, 2009

Keywords: PMMA, dynamic optimization, PDE, sheet reactor

Correspondence concerning this article should be addressed to A. Flores-Tlacuahuac at antonio.flores@uia.mx.

Introduction

Process optimization has a strategic role in polymer plant operability and economics. The importance of global

economy and high-commercial pressure, demand manufacturing better products reducing capital and operating costs. In the polymerization industry, there is considerable economic incentive to develop optimal operating policies that will produce a polymer product with desired molecular and mechanical properties (e.g., density, melt index, impact strength, rigidity, tensile strength, chemical resistance, thermal stability, etc.), which can be related to the values of measured variables such as molecular weight distributions,[1] temperature, viscosity, etc. It has been widely recognized that the transient operation of processing equipment can be improved by the use of optimal dynamic operating policies.[2] Up to now, most of the dynamic optimization techniques applications have been aimed at examining the optimal transient behavior of lumped parameter systems. As computing power and better large scale nonlinear solvers become available one of the natural next steps consists in addressing the optimal dynamic behavior of distributed parameter systems[3] such as the force-circulated warm air reactor addressed in this work.

For medium to large scale systems, two optimal control methodologies dominate the numerical solution of optimal control problems. On one hand, the set of differential and algebraic equations (DAE) comprising the dynamic mathematical model of the addressed system is subject to partial discretization of the output variables and the resulting differential system is numerically integrated.[4] This approach is commonly called the sequential optimal control approach. On the other hand, in the so-called simultaneous approach both the set of manipulated and controlled variables are fully discretized leading to a set of algebraic equations. Therefore, the optimal control problem is transformed into a nonlinear program.[2] Although it has been claimed that the sequential approach is easy to use, it has some disadvantages. Presently, it is unable to handle open-loop unstable systems without previous stabilization. Quite the contrary, it has been shown that the simultaneous approach is able to efficiently handle unstable systems.[5] However, the simultaneous approach demands efficient initialization and bounding strategies and normally state of the art nonlinear solvers able to handle large systems arising from system discretization. However, with ever increasing advances in computing power and the availability of large scale nonlinear optimization solvers, we consider that the simultaneous approach will be widely used for approaching large scale and highly nonlinear optimal control problems. In this work, the simultaneous optimal control approach will be used to address the dynamic optimization of an industrially relevant polymerization reaction engineering problem that features several interesting and challenging problems such as nonlinear behavior and distributed parameter system behavior.

The traditional poly-methylmethacrylate (PMMA) manufacturing process is based on placing plastic sheets inside warm water baths to allow the polymerization reactions to proceed until monomer and initiators are exhausted. However, industrial experience indicates that the quality of the PMMA plastic sheets tends to feature wide variations in molecular weight distributions because of nonuniform heating patterns. Nonuniform polymer properties should be avoided because they give rise to a product featuring undesired quality characteristics (i.e., measured in terms of molecular weight distributions). Therefore, during the PMMA cell-cast process homogenous polymer properties should be promoted. To achieve uniform polymerization properties, it has been recommended to carry out the PMMA polymerization process using a reactor configuration, where heating is provided by force-circulated warm air. Pilot plant tests indicate that better uniform molecular weight distributions could be achieved, especially when compared with the traditional warming bath manufacturing process. In pilot plant experiments,[6] we have observed that even operating the new reactor configuration under isothermal conditions, improved homogenous polymer properties were achieved. This observation led us to conclude that to maximize homogenous polymer properties, dynamic optimal warm air temperature profiles should be used. In this work, our aim is to determine dynamic optimal heating policies able to produce PMMA plastic sheets featuring uniform molecular weight distributions. We claim that optimal heating temperature profiles will lead to homogenous polymer properties.

In a previous work,[6] we proposed a dynamic two-dimensional mathematic model able to reproduce the industrial dynamic behavior of the cell-cast PMMA process. The model response was validated against experimental pilot plant data. Good agreement between model response and experimental plant data was observed. The dynamic model was cast in terms of a two-dimensional PDE system, whose numerical solution was addressed using the method of lines giving rise to a system of ordinary differential equations. The model considered bulk mass free radicals MMA polymerization kinetics and heat conduction transport in the polymerization mixture. This work shows a dynamic optimization model, which uses that model to compute optimal temperature trajectories that can ensure the satisfaction of the product quality (e.g., molecular weight averages). The objective function for this model is composed of three factors such as monomer temperature, air temperature, and weight average molecular weight. Some authors[7,8] use the polydispersity for the optimization, however, according to our industrial experience with the MMA cell cast process, to ensure good plastic sheet properties, temperature, and weight average molecular weight ought to be regulated around desired target values. For the constraints, given by the set of mass and energy balances, the resulting differential system was further time discretized using orthogonal collocation on finite elements, which gave rise to a nonlinear programming problem. A local optimal solution was sought using the IPOPT NLP solver[9] embedded in the AMPL algebraic optimization framework.[10] As far as we know, there are no published works addressing the dynamic optimization of PMMA cell-cast processes taking place in force-circulated warm air reactors.

Cell-Cast Manufacturing Process

Process description

As seen in Figure 1a, in the typical acrilic sheet casting process monomer and small amounts of initiators react in a semibatch reaction system, where a prepolymerization step takes place. The aim of the prepolymerization step is to mix the reactants, to remove the inhibitors normally contained in

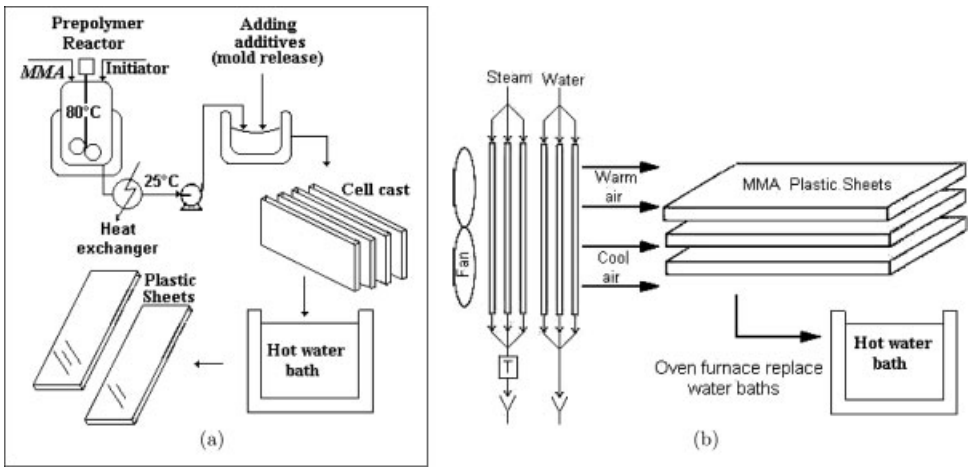

Figure 1. (a) Traditional plastic sheet production flowsheet, and (b) alternative reactor configuration for PMMA polymerization.

commercial MMA and to increase polymer viscosity such that the resulting prepolymerized mixture can be placed between glass plates. Normally, in the prepolymerization step only modest monomer conversion values (around 15-20%) are obtained. After placing the prepolymerized viscous liquid within casting molds, the polymerization is carried out by heating the molds. Heat is provided to the molds by inserting them inside warm water baths. It has been reported[11,12] that this process tends to produce nonuniform plastic sheets (i.e., measured in terms of molecular weight distributions) because polymerization does not take place at the same rate in all parts of the plastic sheet. Monomer temperature variation is perhaps the main reason to explain polymer properties nonuniformity. Therefore, tight control of the operating conditions should help to diminish the polymer properties nonhomogeneity characteristics. Moreover, the aforementioned traditional MMA polymerization process using warm water baths features some shortcomings that could not be lowered by using even advanced control systems. Therefore, recently there has been interest in devising new and efficient plastic sheet polymerization processes featuring better homogeneous polymer properties. An interesting variation of the MMA polymerization process described earlier consists in using a reactor configuration like the one shown in Figure 1b, where heat is provided by force-circulated warm air. Using the force-circulated warm air reactor for plastic sheet production, MMA homogeneous polymer properties could be more easily enforced. A heating profile along the plastic sheet could be imposed and tracked by a control system. In pilot plant experiments,[6] it has been found that this type of polymerization reactors, when properly operated, increase MMA homogenous polymer properties characteristics and reduce the operating time allowed for complete polymerization. Moreover, temperature profile variations are faster and easier to achieve when using air rather than water as heating medium. This operating aspect becomes important if an online control system is used for quality control, especially for temperature profile variations required to manufacture plastic sheets of widely different widths.

Kinetic model

Besides chemical kinetics, physical phenomena related to the diffusion of various chemical reactive species is important in free-radical polymerization reactions. In fact, at high monomer conversions, almost all elementary reactions can become diffusion controlled. Reactions which are influenced by diffusion phenomena include termination of live macroradicals,[13] propagation of a growing chain, and chemical initiation reactions. Diffusion-controlled termination, propagation, and initiation reactions have been related to the gel, glass, and cage effects. In the past 30 years, several models have been published dealing with the mathematical description of diffusion-controlled kinetic rate constants in free-radical polymerization.[14] The reaction mechanism adopted here consists of a simple approximation of the well know bulk free-radical polymerization kinetics featuring straightforward initiation, propagation, chain transfer to monomer, and termination reactions. Although there are more complete kinetics polymerization models proposed in the literature,[15] we found that the model proposed in Ref. 16 was enough to reproduce the experimental pilot plant data for the PMMA plastic sheet[6] polymerization system. The kinetic mechanism of a chemically initiated free-radical polymerization can be described in terms of the following elementary reactions[17]:

Initiation:

$$I \xrightarrow{k} 2R^{\bullet}$$

$$R^{\bullet} + M \xrightarrow{k_i} R_1$$

Propagation:

$$R_n + M \xrightarrow{k_p} R_{n+1}$$

Chain transfer to monomer:

$$R_n + M \xrightarrow{k_f} P_n + R_1$$

Termination by disproportionation:

$$R_n + R_m \xrightarrow{k_{td}} P_n + P_m$$

Termination by combination:

$$R_n + R_m \xrightarrow{k_{td}} P_{n+m}$$

The initiation reaction involves the decomposition of the initiator, I, to produce radicals $R^{\bullet}$, reacting with the monomer molecules, M, to initiate new live (radical) polymer chains R_1. During the propagation step, monomer molecules are added to the live-polymer chains, R_n and R_m. The growth of the chains terminates when the propagating radicals lose their activity through either of the termination reactions, resulting in dead-polymer chains, P_n, P_m, and P_{n+m}.

Plastic sheet PMMA mathematical model

The plastic sheet polymerization mathematical model was derived assuming that the heating source resulting from polymer reaction is a function of the local temperature and reactant/product concentration. It was also assumed that polymer properties changed along the thickness (x-axis) and length (z-axis) of the plastic sheet as depicted in Figure 2. Hence polymer properties were taken as constants along the y-axis. For simplicity, the glass plates are considered homogeneous and isotropic, i.e., the properties are the same in all directions (thermal conductivity, heat capacity, density), average values were taken for MMA and PMMA. To get the two-dimensional dynamic energy balance, the total heat entering and leaving at the x- and z-coordinates was modeled by the Fourier law and the rate of change of energy within the control volume was obtained by applying the shell energy balance method.[18] Because of symmetry considerations, only half of the sheet thickness (from the center to the external surface) was taken into account. Dynamic mass and energy balances coupled through polymerization kinetics[17] describe polymer conversion and molecular weights time evolution. Within the reactor, forced convection warm air provides the required energy to rise up the plastic sheet temperature until a point where significant polymerization rates take place. Within the polymer, the dominant heat transfer mechanism is conduction. Therefore, heat is transferred along the x- and z-axes giving rise to the following two-dimensional dynamic heat transfer equation:

$$\frac{\partial T}{\partial t} = \alpha\left(\frac{\partial^2 T}{\partial x^2} + \frac{\partial^2 T}{\partial z^2}\right) + \frac{Q_{rxn}}{\rho C_p} \tag{1}$$

where T is the polymer temperature, t is the polymerization time, x is the axis of the sheet thickness, z is the axis for the sheet length, ρ is the density, C_p is the heat capacity, α is the thermal diffusivity, and Q_{rxn} stands for the polymerization heat of reaction. The solution domain will be divided into a series of nodes (i.e., the discretization points). At each one of these nodes, the mass balance equations read as follows:

$$\frac{dI}{dt} = -k_d I - \frac{\varepsilon I}{1+\varepsilon X}\lambda_0(k_p + k_f)(1-X) \tag{2a}$$

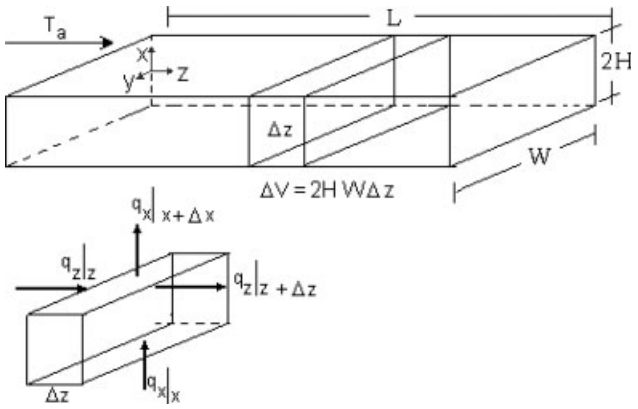

Figure 2. Control volume for energy balance.

T_a is the warming air temperature, H is the thickness, L is the length, W is the width, and q is the amount of heat transferred along each direction.

$$\frac{dX}{dt} = \lambda_0(k_p + k_f)(1-X) \tag{2b}$$

$$\frac{d\lambda_0}{dt} = -\frac{\varepsilon\lambda_0^2}{1+\varepsilon X}(k_p + k_f)(1-X) + 2fk_d I - k_t\lambda_0^2 \tag{2c}$$

$$\frac{d\lambda_1}{dt} = -\frac{\varepsilon\lambda_1\lambda_0}{1+\varepsilon X}(k_p + k_f)(1-X) + 2fk_d I - k_t\lambda_0\lambda_1 + (k_p + k_f)\lambda_0 M_0\frac{1-X}{1+\varepsilon X} \tag{2d}$$

$$\frac{d\lambda_2}{dt} = -\frac{\varepsilon\lambda_2\lambda_0}{1+\varepsilon X}(k_p + k_f)(1-X) + 2fk_d I - k_t\lambda_0\lambda_2 + k_p M_0\frac{1-X}{1+\varepsilon X}(2\lambda_1 + \lambda_0) \tag{2e}$$

$$\frac{d\mu_0}{dt} = -\frac{\varepsilon\mu_0\lambda_0}{1+\varepsilon X}(k_p + k_f)(1-X) + k_{td}\lambda_0^2 + \frac{1}{2}k_{tc}\lambda_0^2 \tag{2f}$$

$$\frac{d\mu_1}{dt} = -\frac{\varepsilon\mu_1\lambda_0}{1+\varepsilon X}(k_p + k_f)(1-X) + k_{td}\lambda_0\lambda_1 + k_{tc}\lambda_0\lambda_1 \tag{2g}$$

$$\frac{d\mu_2}{dt} = -\frac{\varepsilon\mu_2\lambda_0}{1+\varepsilon X}(k_p + k_f)(1-X) + k_{td}\lambda_0\lambda_2 + k_{tc}(\lambda_2\lambda_0 + \lambda_1^2) \tag{2h}$$

The initial (IC) and boundary (BC) conditions of the model are given by

$$\begin{aligned} \text{IC}: t = 0 \quad & T = T_0 \\ & I = I_0, \quad X = X_0, \\ & \lambda_0 = \lambda_{0_0}, \quad \lambda_1 = \lambda_{1_0}, \quad \lambda_2 = \lambda_{2_0}, \\ & \mu_0 = \mu_{0_0}, \quad \mu_1 = \mu_{1_0}, \quad \mu_2 = \mu_{2_0}, \\ & \forall x \in [0, H], \quad z \in [0, L] \end{aligned} \tag{3a}$$

$$\text{BC1}: x = 0 \quad \frac{\partial T}{\partial x} = 0 \tag{3b}$$

$$\text{BC2}: x = H \quad -k\frac{\partial T}{\partial x} = h_a(T - T_a), \quad \forall z \in [0, L] \tag{3c}$$

$$\text{BC3}: z = 0 \quad -k\frac{\partial T}{\partial z} = h_a(T - T_a) \tag{3d}$$

$$\text{BC4}: z = L \quad \frac{\partial T}{\partial z} = 0, \quad \forall x \in [0, H] \tag{3e}$$

where T_0 and M_0 are initial temperature and monomer concentration, respectively, T_a is the warming air temperature, X is the monomer conversion, $\lambda_0, \lambda_1,$ and λ_2 are the zeroth-, first-, and second order moments of growing radical distribution, respectively, whereas $\mu_0, \mu_1,$ and μ_2 are the zeroth-, first- and second-order moments of dead polymer, respectively. The subindex o on λ_i and $\mu_i, i = 0, 2, 3$ stands for initial values of these variables. I is the initiator concentration, k is the monomer average thermal conductivity, f is the initiator efficiency, ε is the volume expansion factor, h_a is the heat transfer coefficient, $k_d, k_p,$ and k_t are the kinetic coefficients for initiation, propagation, and termination steps, respectively. Following we explain with detail the meaning of each boundary condition.

• BC1. We have assumed that the system temperature reaches its maximum value because of symmetry conditions. Hence,

$$\frac{\partial T}{\partial x} = 0$$

• BC2. At the system surface, the temperature is governed by interface transport and it is given by the Fourier heat conduction law and the well known Newton's law of cooling. Therefore,

$$-k\frac{\partial T}{\partial x} = h_a(T - T_a), \quad \forall z \in [0, L]$$

• BC3. This equation simply states the continuity of the flux of heat. Before reaching this point the flux heat is governed by convective transport, when hitting the glass surface the heat flux equation is governed by conductive transport. At the system interphase ($z = 0$) a steady-state energy balance states the conservation of the system energy: heat transported by convection ought to be equal to the energy transported by conduction. Hence,

$$-k\frac{\partial T}{\partial z} = h_a(T - T_a)$$

• BC4. In this point, the glass surface is insulated from the environment, so no heat is transported from this point into the surroundings. Hence,

$$\frac{\partial T}{\partial z} = 0, \quad \forall x \in [0, H]$$

To obtain the full chain-length distribution of the polymer, a very large number of mass balances must be solved. In practice, however, it is sufficient to calculate only the leading moments of the chain-length distribution, where the k-th moment of the live-radical (λ_k) and dead-radical (μ_k) chain-length distributions are defined, respectively, as

$$\lambda_k = \sum_{n=1}^{\infty} n^k R_n, \quad \mu_k = \sum_{n=1}^{\infty} n^k P_n, \quad k = 0, 1, 2$$

average molecular weights (M_n, M_w) were calculated from the leading moments trough the following equations:

$$M_n = \left(\frac{\mu_1 + \lambda_1}{\mu_0 + \lambda_0}\right) M_w^m, \quad M_w = \left(\frac{\mu_2 + \lambda_2}{\mu_1 + \lambda_1}\right) M_w^m$$

where M_w^m is the monomer molecular weight.

In deriving the mathematical model, we assumed that the diffusional mass effect was negligible when compared against diffusional thermal effects. The assumption is a reasonable one for this system in which competing transport processes occur. This may be demonstrated by examining the magnitude of the ratio of the thermal to mass diffusivities (as measured by the Lewis number). If the dimensionless Lewis number (Le) is defined as Le = thermal diffusivity/mass diffusivity = α_{avg}/D_{avg}, and the physical properties, like density, heat capacity, thermal conductivity, and diffusion coefficient are taken as average values for MMA and PMMA at temperature range from 298 to 400 K, then the Lewis number can range from about 6 to 3200. Hence, it becomes clear that the thermal diffusivity has a stronger influence on systems behavior, and this is the main reason why mass diffusivity effects were neglected.

The aforementioned mathematical model features a wide variation in the numerical values of some system states spanning several orders of magnitude. To improve the numerical robustness of the model, and to reduce potential difficulties related to the numerical integration and optimization, the model was properly scaled. The dimensionless variables are defined as follows:

$$\tau = \frac{\alpha t}{H^2}, \quad \xi = \frac{x}{H}, \quad \zeta = \frac{z}{L}$$
$$\theta = \frac{T}{T_0}, \quad \theta_a = \frac{T_a}{T_0}, \quad \bar{I} = \frac{I}{I_0},$$
$$\bar{\lambda}_k = \ln(\lambda_k), \quad \bar{\mu}_k = \ln(\mu_k), \quad k = 0, 1, 2$$

the set of mass and energy balances (at each discretized point) are written in dimensionless form as:

$$\frac{\partial \theta}{\partial \tau} = \frac{\partial^2 \theta}{\partial \xi^2} + a^2\frac{\partial^2 \theta}{\partial \zeta^2} + A_2\bar{Q} \tag{4}$$

$$\frac{d\bar{I}}{d\tau} = -A_1\bar{k}_d\bar{I} - A_1(\bar{k}_p + \bar{k}_f)\varepsilon\bar{I}\frac{1 - X}{1 + \varepsilon X}e^{\bar{\lambda}_0} \tag{5a}$$

$$\frac{dX}{dt} = A_1(\bar{k}_p + \bar{k}_f)(1 - X)e^{\bar{\lambda}_0} \tag{5b}$$

$$\frac{d\bar{\lambda}_0}{d\tau} = -A_1(\bar{k}_p + \bar{k}_f)\varepsilon\frac{1 - X}{1 + \varepsilon X}e^{\bar{\lambda}_0} + A_3\bar{k}_d\bar{I}e^{-\bar{\lambda}_0} - \bar{k}_t e^{\bar{\lambda}_0} \tag{5c}$$

$$\frac{d\bar{\lambda}_1}{d\tau} = -A_1(\bar{k}_p + \bar{k}_f)\varepsilon\frac{1-X}{1+\varepsilon X}e^{\bar{\lambda}_1} + A_3\bar{k}_d\bar{I}e^{-\bar{\lambda}_1} - A_1\bar{k}_t e^{\bar{\lambda}_0} + A_4(\bar{k}_p + \bar{k}_f)\frac{1-X}{1+\varepsilon X}e^{\bar{\lambda}_0-\bar{\lambda}_1} \quad (5d)$$

$$\frac{d\bar{\lambda}_2}{d\tau} = -A_1(\bar{k}_p + \bar{k}_f)\varepsilon\frac{1-X}{1+\varepsilon X}e^{\bar{\lambda}_0} + A_3\bar{k}_d\bar{I}e^{\bar{\lambda}_1} - A_1\bar{k}_t e^{\bar{\lambda}_0} + A_4(\bar{k}_p + \bar{k}_f)\frac{1-X}{1+\varepsilon X}(2e^{\bar{\lambda}_1-\bar{\lambda}_2} + e^{\bar{\lambda}_0-\bar{\lambda}_2}) \quad (5e)$$

$$\frac{d\bar{\mu}_0}{d\tau} = -A_1\left[(\bar{k}_p+\bar{k}_f)\varepsilon\frac{1+X}{1+\varepsilon X}e^{\bar{\lambda}_0} + \left(\bar{k}_{td} + \frac{1}{2}\bar{k}_{tc}\right)e^{2\bar{\lambda}_0-\bar{\mu}_0}\right] \quad (5f)$$

$$\frac{d\bar{\mu}_1}{d\tau} = -A_1\left[(\bar{k}_p + \bar{k}_f)\varepsilon\frac{1-X}{1+\varepsilon X}e^{\bar{\lambda}_0} + \bar{k}_t e^{\bar{\lambda}_0+\bar{\lambda}_1-\bar{\mu}_1}\right] \quad (5g)$$

$$\frac{d\bar{\mu}_2}{d\tau} = -A_1\left[(\bar{k}_p + \bar{k}_f)\varepsilon\frac{1-X}{1+\varepsilon X}e^{\bar{\lambda}_0} + \bar{k}_{td}e^{\bar{\lambda}_0+\bar{\lambda}_2-\bar{\mu}_2} + \bar{k}_{tc}(e^{\bar{\lambda}_2+\bar{\lambda}_0-\bar{\mu}_2} + e^{2\bar{\lambda}_1-\bar{\mu}_2})\right] \quad (5h)$$

whereas the dimensionless initial and boundary conditions read as follows:

$$\text{IC1} : \tau = 0 \quad \theta = \theta_0, \quad \bar{I} = 1, \quad X = X_0, \quad \bar{\lambda}_0 = \ln(\lambda_{0_0}), \quad \bar{\lambda}_1 = \ln(\lambda_{1_0}), \quad \bar{\lambda}_2 = \ln(\lambda_{2_0}), \quad \bar{\mu}_0 = \ln(\mu_{0_0}), \quad \bar{\mu}_1 = \ln(\mu_{1_0}), \quad \bar{\mu}_2 = \ln(\mu_{2_0}), \quad \forall\xi \in [0,1], \quad \zeta \in [0,1] \quad (6a)$$

$$\text{BC1} : \xi = 0 \quad \frac{\partial\theta}{\partial\xi} = 0 \quad (6b)$$

$$\text{BC2} : \xi = 1 \quad \frac{\partial\theta}{\partial\xi} = Bi_x(\theta - \theta_a), \quad \forall\zeta \in [0,1] \quad (6c)$$

$$\text{BC3} : \zeta = 0 \quad \frac{\partial\theta}{\partial\zeta} = Bi_z(\theta - \theta_a) \quad (6d)$$

$$\text{BC4} : \zeta = 1 \quad \frac{\partial\theta}{\partial\zeta} = 0, \quad \forall\xi \in [0,1] \quad (6e)$$

where $Bi_x = hH/k$ and $Bi_z = hL/k$ are the Biot number for x- and z-coordinates, respectively, and $a = H/L$, $A_1 = H^2/\alpha$, $A_2 = H^2(-\Delta H_r)M_0/(kT_0)$, $A_3 = 2fH^2I_0/\alpha$, $A_4 = H^2M_0/\alpha$ are dimensionless constants. In this work, we used the polymerization kinetics and the gel and glass effects models as proposed by Chiu et al.[19] The parameter values are given as follows: $Bi_x = 10.7$, $Bi_z = 535$, $a = 3.3\times10^{-3}$, $A_1 = 1.3392\times10^5$, $A_2 = 0.7807$, $A_3 = 24.0493$, and $A_4 = 1.3392\times10^6$ for 6 mm thickness sheet, and $Bi_x = 32$, $Bi_z = 3210$, $a = 0.01$, $A_1 = 1.2053\times10^6$, $A_2 = 7.0261$, $A_3 = 216.4435$, and $A_4 = 1.2053\times10^7$ for 18 mm thickness sheet. The dimensionless PMMA kinetic rate constants are given by

$$\frac{1}{\bar{k}_p} = \frac{1}{\bar{k}_{p0}} + \Theta_p\exp\left(\bar{\lambda}_0 - \frac{2.3\phi_m}{A + 0.03\phi_m}\right) \quad (7a)$$

$$\frac{1}{\bar{k}_t} = \frac{1}{\bar{k}_{t0}} + \Theta_t\exp\left(\bar{\lambda}_0 - \frac{2.3\phi_m}{A + 0.03\phi_m}\right) \quad (7b)$$

$$\Theta_p = 5.4814\times10^{-16}\exp\left(\frac{13982}{T_0\theta}\right) \quad (7c)$$

$$\Theta_t = \frac{1.1353\times10^{-22}}{I_0}\exp\left(\frac{17420}{T_0\theta}\right) \quad (7d)$$

$$A = -8.0\times10^{-6}T_0^2(\theta - \theta_g)^2 + 0.1678 \quad (7e)$$

$$\bar{k}_{p0} = 2.95\times10^7\exp\left(-\frac{2190.5}{T_0\theta}\right) \quad (7f)$$

$$\bar{k}_{t0} = 5.88\times10^9\exp\left(-\frac{352.8}{T_0\theta}\right) \quad (7g)$$

$$\bar{k}_d = 6.32\times10^{16}\exp\left(-\frac{15398.6}{T_0\theta}\right) \quad (7h)$$

$$\phi_m = \frac{1-X}{1+\varepsilon X} \quad (7i)$$

$$\bar{k}_t = \bar{k}_{tc} + \bar{k}_{td} \quad (7j)$$

$$\bar{k}_{td} = \bar{k}_t \Big/ \left[1 + 3.956\times10^{-4}\exp\left(\frac{2058.2}{T_0\theta}\right)\right] \quad (7k)$$

$$\bar{k}_f = \bar{k}_t \Big/ \left[1 + 3.956\times10^{-4}\exp\left(\frac{2058.2}{T_0\theta}\right)\right] \quad (7l)$$

where $B = 0.03$ is the parameter in the Fujita–Doolittle equation[20] and $\theta_g = 1.198$ is the dimensionless glass transition temperature, respectively.

It should be stressed that due to significant volume contraction of PMMA with respect to MMA (around 20%), strictly speaking the polymerization process features true moving boundary behavior. However, introducing moving boundaries might lead to a problem complex to solve. One

of our aims was to keep both the problem formulation and solution as simple as possible. The justification for using fixed boundaries was the realization that even using fixed boundaries our numerical results seem to match the available experimental industrial information. In fact, in a previous publication,[6] we shown a comparison of experimental pilot plant results versus simulation ones for two different thicknesses (3 and 6 mm) of the plastic sheet. Comparison against experimental data shows that the prediction capabilities of the proposed model seem to be satisfactory for industrial application, especially for small thickness plastic sheets. From Figure 12 of the aforementioned publication, it can be observed that the shrinkage is homogenous for 3 and 6 mm thickness plastic sheets. However, higher deviation are observed for 12 and 18 mm thickness plastic sheets. Even in this last case, deviations are not too large (around 4%). These observations support our decision of addressing the polymer contraction behavior as a fixed boundary problem. Moreover, volume contraction was taken into account by: $V = V_o(1 + \varepsilon X)$, where ε is the volume contraction factor and computed from: $\varepsilon = (\rho_m - \rho_p)/\rho_p$, where ρ_m and ρ_p are the monomer and polymer densities, respectively.

Dynamic Optimization

The mechanical properties of polymers have been shown to strongly depend on the molecular weight distribution (MWD). Typical goals in operating a polymerization reactor are to minimize polydispersity or the number molecular weight distribution to produce a polymer featuring target mechanical and rheological properties.[21] Nunes et al.[21] found that thermal properties, stress-strain properties, impact resistance, strength and hardness of films of polymethyl methacrylate, and polystyrene were all improved by narrowing the MWD. Hence, the development of a methodology for adjusting the MWD in the manufacturing of MMA plastic sheets should lead to a polymer with improved target properties. Depending on the intended use of the polymer product, polymers with various types of MWD are required.[22] Experimentally, it has been observed that homogeneous polymer properties in the MMA cell cast process can be promoted by proper selection of warming air temperature profiles. Because the MMA cell cast process is essentially a batch process, most of the related polymer properties strongly depend on the time variation of operating parameters (i.e., warming air temperature). Therefore, the dynamic optimal operation of the reactor should lead to a better and improved MMA homogenous polymerization system. We propose a dynamic optimization formulation whose objective is to determine dynamic optimal heating patterns leading to homogeneous and improved plastic sheet properties.

To compute optimal dynamic heating profiles, we use the following objective function:

$$\min_{\theta_a, x} \int_0^{\tau} \left[\left(1 - \frac{\theta}{\theta^d}\right)^2 + \left(1 - \frac{\theta_a}{\theta_a^d}\right)^2 + \left(1 - \frac{M_w}{M_w^d}\right)^2 \right] d\tau \qquad (8)$$

In the above equation θ^d, θ_a^d, and M_w^d stand for the desired values of dimensionless monomer temperature, dimensionless air temperature, and weight average molecular weight, respectively, whereas $\mathbf{x}$ is the vector of system states. Our aim is to compute the dimensionless warming air temperature as time function $\theta_a(t)$ so to drive the plastic sheet dimensionless temperature θ to its desired profile as soon as possible while meeting a set of process constraints.

Even when at first glance, polymer polydispersity seems a variable whose value should be regulated, we decided not to consider it as decision variable. Polydispersity is a variable that sometimes might reflect desired product quality (as in some polymerization batch systems). However, according to our industrial experience with the MMA cell cast process, to ensure good plastic sheet properties, temperature, and weight average molecular weight ought to be regulated around desired target values. We have observed that when the plastic sheet features those properties values, polydispersity can range between 2 and 4, and even so the plastic sheet properties are the required ones. This is the reason why polydispersity was not considered as a decision variable in our optimization formulation: its inclusion is not strictly required to enforce target properties of the MMA plastic sheet.

Using the simultaneous approach for solving the dynamic optimization problem, given by the objective function (Eq. 8) and the model and operating constraints (Eqs. 4–6e), amounts to transform the original dynamic optimization problem into a nonlinear program (NLP). The transformation involves two steps: (a) the method of lines[23] was used to take care of the spatial coordinates transforming the original PDAE system into a system of ordinary differential equations (ODE), and (b) orthogonal collocation on finite elements was used to transform the ODE system into a set of nonlinear algebraic equations.[2] The integral term in the objective function was approximated by a Radau cuadrature. The discretized NLP problem is given by the following objective function:

$$\min_{\theta_{a_{mk}}} \sum_{m=1}^{N_e} \Delta\tau_m \sum_{k=1}^{N_c} \left[\sum_{i=1}^{N_x} \sum_{j=1}^{N_z} \left(1 - \frac{\theta_{mkij}}{\theta^d}\right)^2 + \left(1 - \frac{\theta_{a_{mk}}}{\theta_a^d}\right)^2 + \left(1 - \frac{M_{w_{mkij}}}{M_w^d}\right)^2 \right] \qquad (9)$$

where θ_{mkij} denotes the value of dimensionless temperature at the m-th finite element, k is the collocation point within that element, i is the position point for the sheet thickness (x-axis), and j is the position point for the sheet length (z-axis). N_e is the number of finite elements, N_c is the number of collocation points, N_x and N_z are the number of points for discretization along the x- and z-coordinates, respectively, whereas $\Delta\tau_m$ is the length of m-th finite element.

The dynamic optimization formulation is subject to the following set of discretized constraints. The dimensionless temperature approximation is given by the following Lagrange polynomial interpolation:

$$\theta_{mkij} = \theta_{mij}^0 + \Delta\tau_m \tau_{tr} \sum_{n=1}^{Nc} A_{nk} \dot{\theta}_{mnij} \qquad (10)$$

where θ_{mij}^0 is the temperature at the starting point of each element, and τ_{tr} is the operating time. The temperature continuity between finite elements is enforced trough the following constraint:

$$\theta^0_{mij} = \theta^0_{m-1ij} + \Delta\tau_{m-1}\tau_{tr}\sum_{n=1}^{Nc} A_{nNc}\dot{\theta}_{m-1nij} \tag{11}$$

The discretized energy balance is given by the following equation:

$$\dot{\theta}_{mnij} = \frac{1}{\Delta\zeta^2}(\theta_{mni+1j} - 2\theta_{mnij} + \theta_{mni-1j}) + \frac{a^2}{\Delta\zeta^2}(\theta_{mnij+1} - 2\theta_{mnij} + \theta_{mnij-1}) + A_2\bar{Q}_{mnij} \quad i = 2,3,...,N_x - 1,\ j = 2,3,...,N_z - 1 \tag{12}$$

where $\Delta\zeta$ is the grid spacing for dimensionless length.

The Lagrange interpolated monomer conversion, initiator concentration and the zeroth, first, and second moments of both living and dead polymer chains read as follows:

$$\bar{I}_{mkij} = \bar{I}^0_{mij} + \Delta\tau_m\tau_{\mathrm{tr}}\sum_{n=1}^{Nc} A_{nk}\dot{\bar{I}}_{mnij} \tag{13a}$$

$$X_{mkij} = X^0_{mij} + \Delta\tau_m\tau_{\mathrm{tr}}\sum_{n=1}^{Nc} A_{nk}\dot{X}_{mnij} \tag{13b}$$

$$\bar{\lambda}_{0_{mkij}} = \bar{\lambda}^0_{0_{mij}} + \Delta\tau_m\tau_{\mathrm{tr}}\sum_{n=1}^{Nc} A_{nk}\dot{\bar{\lambda}}_{0_{mnij}} \tag{13c}$$

$$\bar{\lambda}_{1_{mkij}} = \bar{\lambda}^0_{1_{mij}} + \Delta\tau_m\tau_{\mathrm{tr}}\sum_{n=1}^{Nc} A_{nk}\dot{\bar{\lambda}}_{1_{mnij}} \tag{13d}$$

$$\bar{\lambda}_{2_{mkij}} = \bar{\lambda}^0_{2_{mij}} + \Delta\tau_m\tau_{\mathrm{tr}}\sum_{n=1}^{Nc} A_{nk}\dot{\bar{\lambda}}_{2_{mnij}} \tag{13e}$$

$$\bar{\mu}_{0_{mkij}} = \bar{\mu}^0_{0_{mij}} + \Delta\tau_m\tau_{\mathrm{tr}}\sum_{n=1}^{Nc} A_{nk}\dot{\bar{\mu}}_{0_{mnij}} \tag{13f}$$

$$\bar{\mu}_{1_{mkij}} = \bar{\mu}^0_{1_{mij}} + \Delta\tau_m\tau_{\mathrm{tr}}\sum_{n=1}^{Nc} A_{nk}\dot{\bar{\mu}}_{1_{mnij}} \tag{13g}$$

$$\bar{\mu}_{2_{mkij}} = \bar{\mu}^0_{2_{mij}} + \Delta\tau_m\tau_{\mathrm{tr}}\sum_{n=1}^{Nc} A_{nk}\dot{\bar{\mu}}_{2_{mnij}} \tag{13h}$$

where X^0_{mj}, $\bar{\lambda}^0_{0_{mj}}$, and $\bar{I}^0_{mj}$ are evaluated at the starting point of each element. The continuity constraints between adjacent elements are:

$$\bar{I}^0_{mij} = \bar{I}^0_{m-1ij} + \Delta\tau_{m-1}\tau_{\mathrm{tr}}\sum_{n=1}^{Nc} A_{nNc}\dot{\bar{I}}_{m-1nij} \tag{14a}$$

$$X^0_{mij} = X^0_{m-1ij} + \Delta\tau_{m-1}\tau_{\mathrm{tr}}\sum_{n=1}^{Nc} A_{nNc}\dot{X}_{m-1nij} \tag{14b}$$

$$\bar{\lambda}^0_{0_{mij}} = \bar{\lambda}^0_{0_{m-1ij}} + \Delta\tau_{m-1}\tau_{\mathrm{tr}}\sum_{n=1}^{Nc} A_{nNc}\dot{\bar{\lambda}}_{0_{m-1nij}} \tag{14c}$$

$$\bar{\lambda}^0_{1_{mij}} = \bar{\lambda}^0_{1_{m-1ij}} + \Delta\tau_{m-1}\tau_{\mathrm{tr}}\sum_{n=1}^{Nc} A_{nNc}\dot{\bar{\lambda}}_{1_{m-1nij}} \tag{14d}$$

$$\bar{\lambda}^0_{2_{mij}} = \bar{\lambda}^0_{2_{m-1ij}} + \Delta\tau_{m-1}\tau_{\mathrm{tr}}\sum_{n=1}^{Nc} A_{nNc}\dot{\bar{\lambda}}_{2_{m-1nij}} \tag{14e}$$

$$\bar{\mu}^0_{0_{mij}} = \bar{\mu}^0_{0_{m-1ij}} + \Delta\tau_{m-1}\tau_{\mathrm{tr}}\sum_{n=1}^{Nc} A_{nNc}\dot{\bar{\mu}}_{0_{m-1nij}} \tag{14f}$$

$$\bar{\mu}^0_{1_{mij}} = \bar{\mu}^0_{1_{m-1ij}} + \Delta\tau_{m-1}\tau_{\mathrm{tr}}\sum_{n=1}^{Nc} A_{nNc}\dot{\bar{\mu}}_{1_{m-1nij}} \tag{14g}$$

$$\bar{\mu}^0_{2_{mij}} = \bar{\mu}^0_{2_{m-1ij}} + \Delta\tau_{m-1}\tau_{\mathrm{tr}}\sum_{n=1}^{Nc} A_{nNc}\dot{\bar{\mu}}_{2_{m-1nij}} \tag{14h}$$

the starting values are $X^0_{1ij} = X_0$, $\bar{I}^0_{1ij} = 1$, $\bar{\lambda}^0_{0_{1ij}} = \ln(\lambda_0)$, $\bar{\lambda}^0_{1_{1ij}} = \ln(\lambda_1)$, $\bar{\lambda}^0_{2_{1ij}} = \ln(\lambda_2)$, $\bar{\mu}^0_{0_{1ij}} = \ln(\mu_0)$, $\bar{\mu}^0_{1_{1ij}} = \ln(\mu_1)$, $\bar{\mu}^0_{2_{1ij}} = \ln(\mu_2)$, at $i = 1,2,...,N_x$, $j = 1,2,...,N_z$.

The discretized mass balances for the monomer conversion, initiator concentration, and the zeroth, first, and second moments of both living and dead polymer chains are given as follows:

$$\dot{\bar{I}}_{mnij} = -A_1\bar{k}_{d_{mnij}}\bar{I}_{mnij} - A_1(\bar{k}_{\mathrm{p}_{mnij}} + \bar{k}_{\mathrm{f}_{mnij}}) \times \varepsilon_{mnij}\bar{I}_{mnij}\frac{1 - X_{mnij}}{1 + \varepsilon_{mnij}X_{mnij}}e^{\bar{\lambda}_{0_{mnij}}} \tag{15a}$$

$$\dot{X}_{mnij} = A_1(\bar{k}_{\mathrm{p}_{mnij}} + \bar{k}_{\mathrm{f}_{mnij}})(1 - X_{mnij})e^{\bar{\lambda}_{0_{mnij}}} \tag{15b}$$

$$\dot{\bar{\lambda}}_{0_{mnij}} = -A_1(\bar{k}_{\mathrm{p}_{mnij}} + \bar{k}_{\mathrm{f}_{mnij}})\varepsilon_{mnij}\frac{1 - X_{mnij}}{1 + \varepsilon_{mnij}X_{mnij}}e^{\bar{\lambda}_{0_{mnij}}} + A_3\bar{k}_{\mathrm{d}_{mnij}}\bar{I}_{mnij}e^{-\bar{\lambda}_{0_{mnij}}} - \bar{k}_{t_{mnij}}e^{\bar{\lambda}_{0_{mnij}}} \tag{15c}$$

$$\dot{\bar{\lambda}}_{1_{mnij}} = -A_1(\bar{k}_{\mathrm{p}_{mnij}} + \bar{k}_{\mathrm{f}_{mnij}})\varepsilon_{mnij}\frac{1 - X_{mnij}}{1 + \varepsilon_{mnij}X_{mnij}}e^{\bar{\lambda}_{1_{mnij}}} + A_3\bar{k}_{\mathrm{d}_{mnij}}\bar{I}_{mnij}e^{-\bar{\lambda}_{1_{mnij}}} - A_1\bar{k}_{t_{mnij}}e^{\bar{\lambda}_{0_{mnij}}} + A_4(\bar{k}_{\mathrm{p}_{mnij}} + \bar{k}_{\mathrm{f}_{mnij}}) \times \frac{1 - X_{mnij}}{1 + \varepsilon_{mnij}X_{mnij}}e^{\bar{\lambda}_{0_{mnij}} - \bar{\lambda}_{1_{mnij}}} \tag{15d}$$

$$\dot{\bar{\lambda}}_{2_{mnij}} = -A_1(\bar{k}_{p_{mnij}} + \bar{k}_{f_{mnij}})\varepsilon_{mnij}\frac{1 - X_{mnij}}{1 + \varepsilon_{mnij}X_{mnij}}e^{\bar{\lambda}_{0_{mnij}}} + A_3\bar{k}_{d_{mnij}}\bar{I}_{mnij}e^{\bar{\lambda}_{1_{mnij}}} - A_1\bar{k}_{t_{mnij}}e^{\bar{\lambda}_{0_{mnij}}} + A_4(\bar{k}_{p_{mnij}} + \bar{k}_{f_{mnij}}) \times \frac{1 - X_{mnij}}{1 + \varepsilon_{mnij}X_{mnij}}(2e^{\bar{\lambda}_{1_{mnij}} - \bar{\lambda}_{2_{mnij}}} + e^{\bar{\lambda}_{0_{mnij}} - \bar{\lambda}_{2_{mnij}}}) \quad (15e)$$

$$\dot{\bar{\mu}}_{0_{mnij}} = -A_1\left[(\bar{k}_{p_{mnij}} + \bar{k}_{f_{mnij}})\varepsilon_{mnij}\frac{1 + X_{mnij}}{1 + \varepsilon_{mnij}X_{mnij}}e^{\bar{\lambda}_{0_{mnij}}} + \left(\bar{k}_{td_{mnij}} + \frac{1}{2}\bar{k}_{tc_{mnij}}\right)e^{2\bar{\lambda}_{0_{mnij}} - \bar{\mu}_{0_{mnij}}}\right] \quad (15f)$$

$$\dot{\bar{\mu}}_{1_{mnij}} = -A_1\left[(\bar{k}_{p_{mnij}} + \bar{k}_{f_{mnij}})\varepsilon_{mnij}\frac{1 - X_{mnij}}{1 + \varepsilon_{mnij}X_{mnij}}e^{\bar{\lambda}_{0_{mnij}}} + \bar{k}_{t_{mnij}}e^{\bar{\lambda}_{0_{mnij}} + \bar{\lambda}_{1_{mnij}} - \bar{\mu}_{1_{mnij}}}\right] \quad (15g)$$

$$\dot{\bar{\mu}}_{2_{mnij}} = -A_1\left[(\bar{k}_{p_{mnij}} + \bar{k}_{f_{mnij}})\varepsilon_{mnij}\frac{1 - X_{mnij}}{1 + \varepsilon_{mnij}X_{mnij}}e^{\bar{\lambda}_{0_{mnij}}} + \bar{k}_{td_{mnij}}e^{\bar{\lambda}_{0_{mnij}} + \bar{\lambda}_{2_{mnij}} - \bar{\mu}_{2_{mnij}}} + \bar{k}_{tc_{mnij}}(e^{\bar{\lambda}_{2_{mnij}} + \bar{\lambda}_{0_{mnij}} - \bar{\mu}_{2_{mnij}}} + e^{2\bar{\lambda}_{1_{mnij}} - \bar{\mu}_{2_{mnij}}})\right] \quad (15h)$$

The following algebraic equations stand for the boundary condition constrains:

$$\frac{-3\theta_{mn1} + 4\theta_{mn2} - \theta_{mn3}}{2\Delta\zeta} + Bi_z(\theta_{mn1} - \theta_{amn}) = 0 \quad (16a)$$

$$4\theta_{mnN_z} - 3\theta_{mnN_z-1} + \theta_{mnN_z-2} = 0 \qquad m = 1, 2, ..., N_e, \;\; n = 1, 2, ..., N_c \quad (16b)$$

Results and Discussion

In this section two types of dynamic optimization problems were addressed: (a) in the first formulation, hereafter denoted by P_1, the objective function of the optimization problem was composed of only the first two terms of Eq. 8 (involving $\theta, \theta^d, \theta_a$, and θ_a^d), and (b) in the second formulation (denoted by P_2) all the three terms (including besides the M_w and M_w^d terms) of the objective function were taken into account. Both P_1 and P_2 formulations are subject to the same set of constraints given by Eqs. 10–16(b). The aim of solving the first formulation lies in determining the optimal heating profile $\theta_a(t)$ such that the plastic sheet temperature θ and the air temperature θ_a feature values as close as possible to their target values. The aim of the P_2 formulation is similar to the P_1 formulation but augmented with the requirement that the weight average molecular weight M_w should be as close as possible to its target value M_w^d. Moreover, to test the advantages of using dynamic optimal warming temperature profiles, the results from solving the first and second optimization formulations were compared against typical simple operating policies (SOP) based on operating the reactor at constant warm air temperature (50°C). From an optimization point of view is clear that the second formulation turns out to be harder to solve that the first one because it involves additional terms in the objective function and because the complex interplay between temperature and weight average molecular weight. For each case, the analysis was done for 6 and 18 mm plastic sheet thicknesses at two different initial warm air temperature values (65 and 78°C). Moreover, because dynamic optimal warming profiles might depend on process uncertainty, in this section, the effect of polymerization kinetics uncertainty on optimal heating profiles was also addressed. Dynamic optimization studies under nominal operating conditions could feature poor performance or even be inoperable because of process uncertainty.

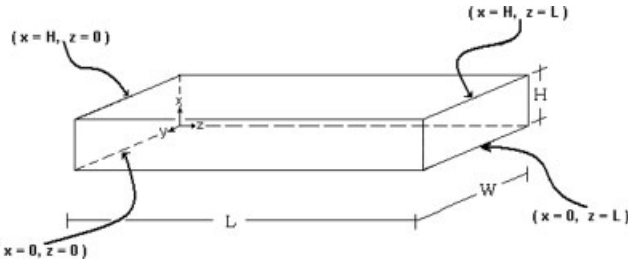

Figure 3. Location of the four places where computed results are reported.

Before presenting the dynamic optimization results it should be remarked that, to get homogeneous polymer properties, pilot plant tests have shown that the plastic sheet temperature should be 50°C during most of the polymerization process. The results of the calculations are only presented for certain points along the sheet. The reason for doing so is because experimentally it is easier to measure the plastic sheet temperature in those places. Accordingly, the results are presented for four point along the plastic sheet. As shown in Figure 3 the results are reported at the following points: [$x = 0$, $z = 0$], [$x = H$, $z = 0$], [$x = 0$, $z = L$] and [$x = H$, $z = L$]. Dynamic optimal results will be represented by a solid (—) and dashed (−−) lines at $x = 0$ and $x = H$, respectively, for either $z = 0$ or $z = L$. Dynamic optimal results will be compared against SOP results that will be represented by dotted (···) and dash-dot (-.) lines at $x = 0$ and $x = H$, respectively, for either $z = 0$ and $z = L$. In Figures 4–11, the subscript on x, either P_1, P_2 or SOP, stands for results computed using the P_1 or P_2 formulations or results obtained using the simple operating policies SOP, respectively. Finally, the warming air temperature dynamic optimal profile (i.e. the manipulated variable) is also shown. For reading facility we have decided to plot the optimal manipulated variable profile from right to left.

Table 1 contains the design data for the PMMA plastic sheet reactor as well the target or desired values of the plastic sheet and warm air temperatures and the molecular weight distribution appearing in the objective function, whereas Table 2 displays information regarding features related to the numerical solution of the underlying NLP problem such as the number of discrete points along the x

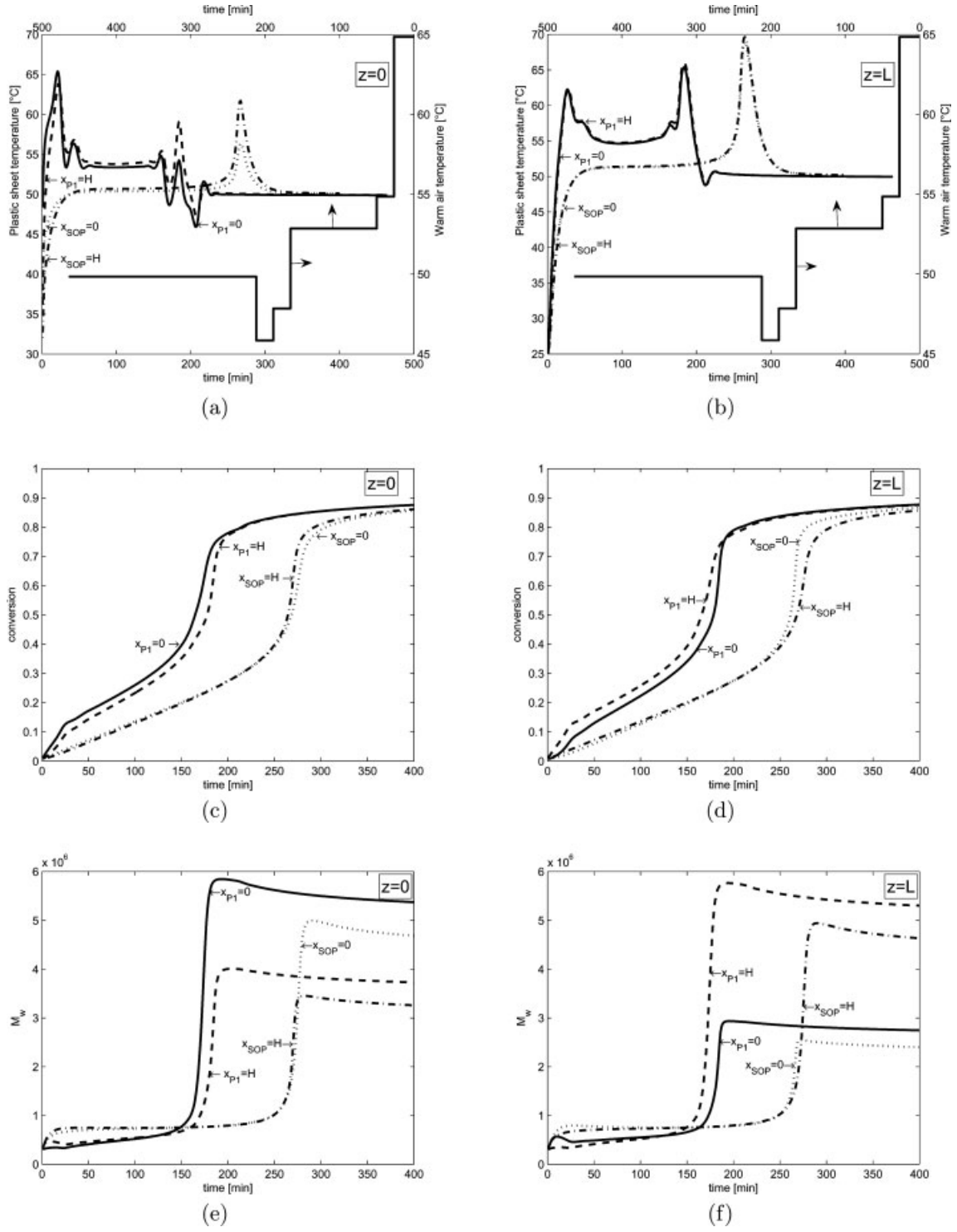

Figure 4. Case 1. Monomer temperature, conversion, and weight average molecular weight dynamic optimal responses and comparison against SOP results for P_1 formulation, 6 mm thickness, and 65°C initial air temperature.

The stairs line stands for the warm air optimal profile.

and z directions, the number of finite elements and CPU solution statistics. In all cases three internal collocation points were used. The numerical results for all cases were obtained on a Pentium IV computer with 2.8 GHz clock speed and 512 KB RAM. The optimization formulations were solved using the IPOPT NLP solver[9] embedded in the AMPL Mathematical Programming environment.[10] In the following section the first variable denotes either the P_1 or P_2

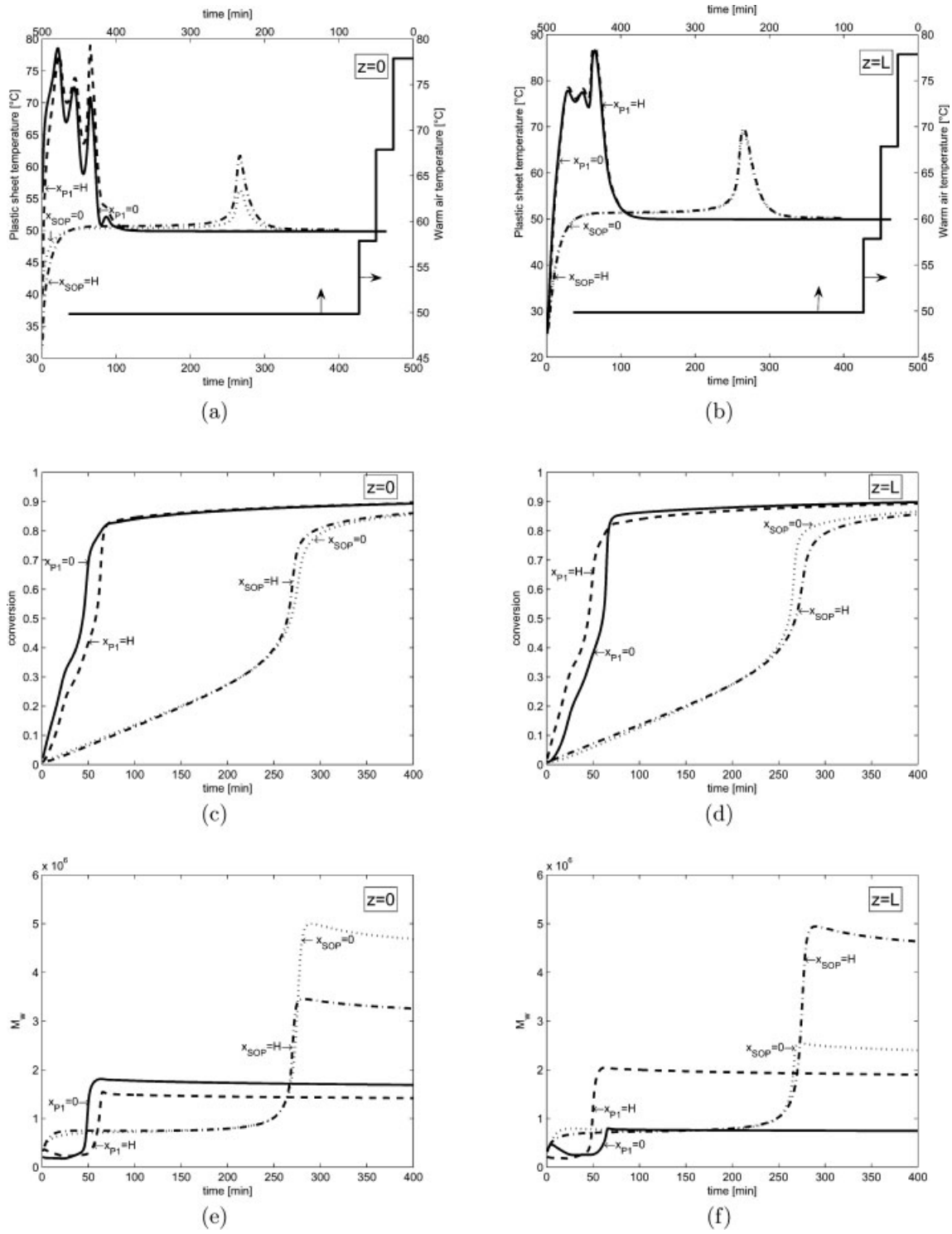

Figure 5. Case 1. Monomer temperature, conversion, and weight average molecular weight dynamic optimal responses and comparison against SOP results for P_1 formulation, 6 mm thickness, and 78°C initial warm air temperature.

The stairs line stands for the warm air optimal profile.

formulations, the second one refers to the thickness of the plastic sheet whereas the last variable denotes the initial values of the warming air temperature.

Case 1: P_1, 6 mm, 65 and 78°C

The dynamic responses for monomer temperature, monomer conversion, and molecular weight distribution are shown

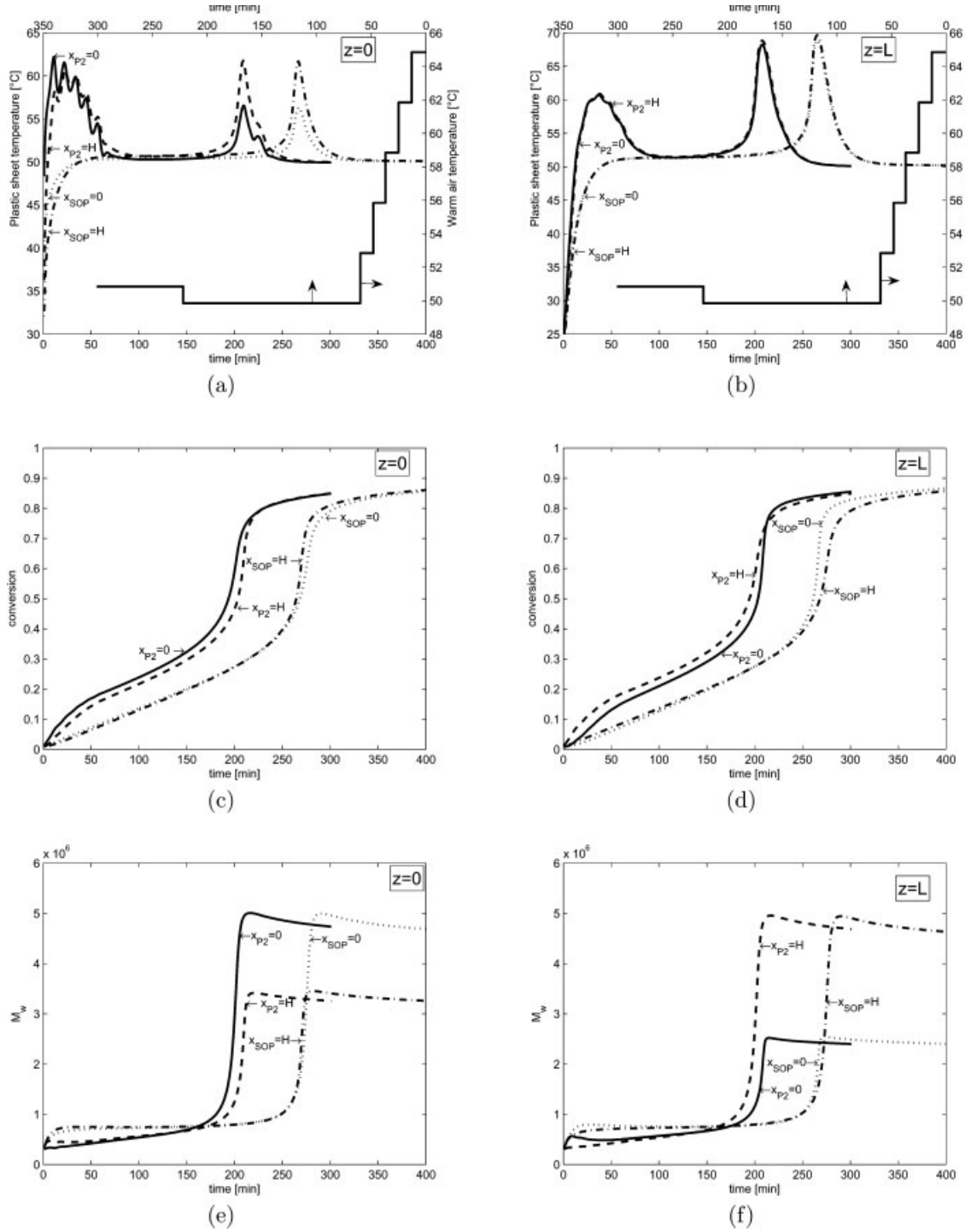

Figure 6. Case 2. Monomer temperature, conversion, and weight average molecular weight dynamic optimal responses and comparison against SOP results for P_2 formulation, 6 mm thickness, and 65°C initial warm air temperature.

The stairs line stands for the warm air optimal profile.

in Figure 4 for a 6 mm thickness plastic sheet. The first column of the figure refers to results at the left side of the sheet, whereas the second column displays results at the right side of the plastic sheet as shown in Figure 3. It should be pointed out that the warm air temperature has been arbitrarily initialized at 65°C.

From Figure 4, we note that dynamic optimal operating policies lead to a reduction of the time required to

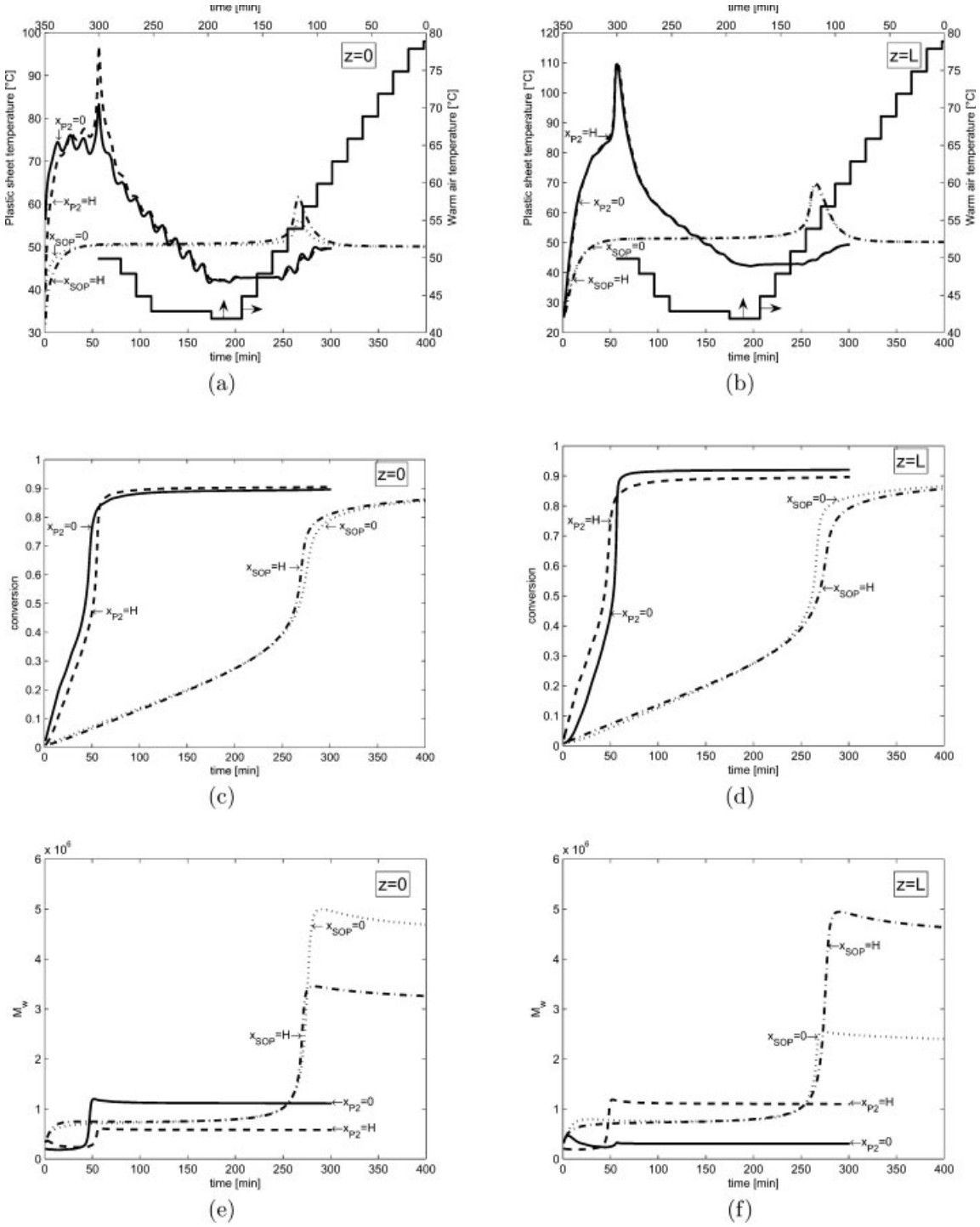

Figure 7. Case 2. Monomer temperature, conversion, and weight average molecular weight dynamic optimal responses and comparison against SOP results for P_2 formulation, 6 mm thickness, and 78°C initial warm air temperature.

The stairs line stands for the warm air optimal profile.

manufacture PMMA plastic sheets. This saving in processing time translates into a reduction of heating utilities resulting in increased process profit. Using the optimal warming temperature profile, the polymerization process has almost finished in around 220 minutes at $z = 0$, whereas using the SOP temperature profile the gel effect has not yet emerged. This tendency is also clearly noted at $z = L$. Moreover, the optimal warming air temperature profile gives rise to a smaller gel effect temperature peak. Because of the small sheet thickness the results at $x = 0$ and $x = H$ are rather

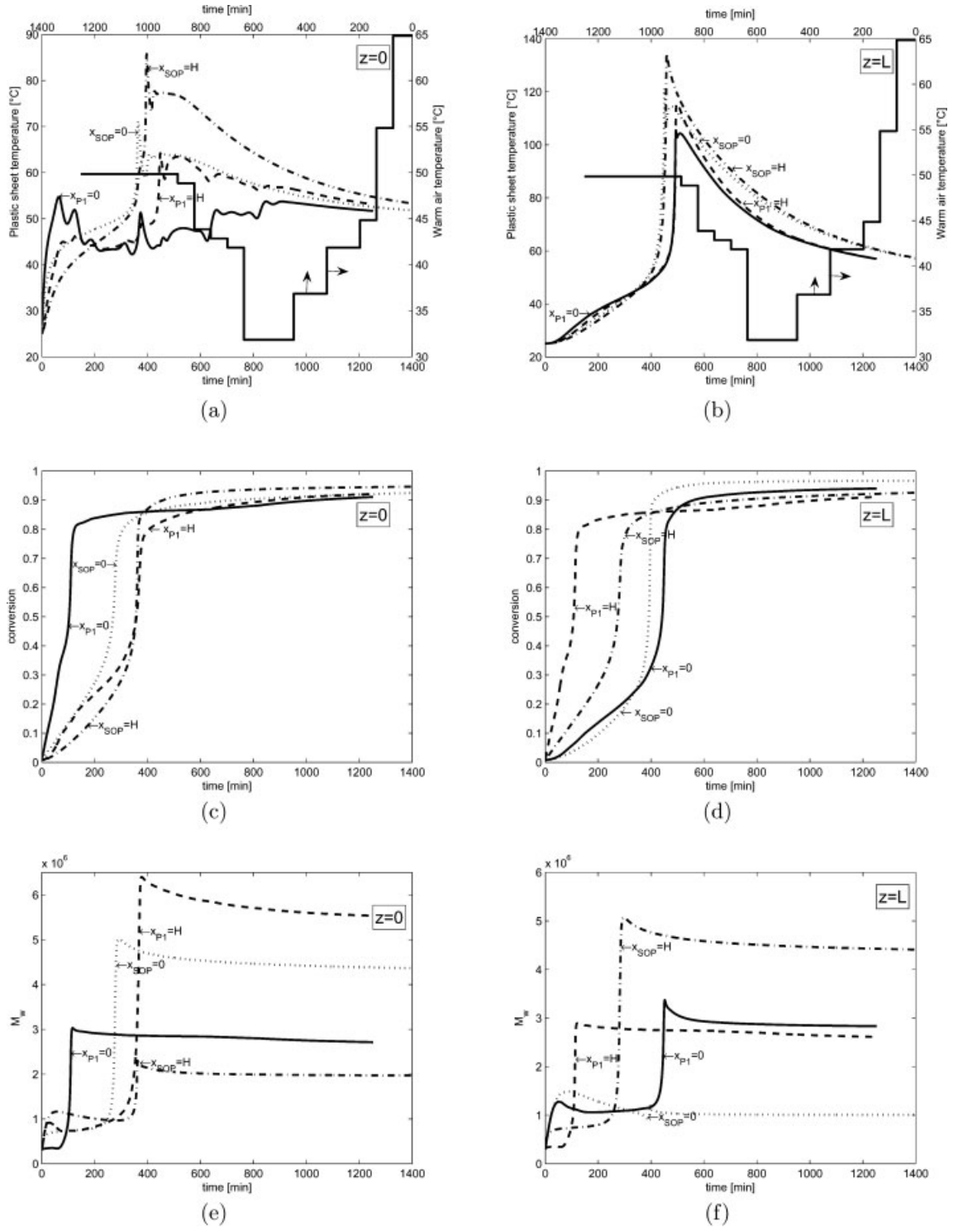

Figure 8. Case 3. Monomer temperature, conversion, and weight average molecular weight dynamic optimal responses and comparison against SOP results for P_1 formulation, 18 mm thickness, and 65°C initial warm air temperature.

The stairs line stands for the warm air optimal profile.

similar for either $z = 0$ and $z = L$. Because in the P_1 formulation, the weight average molecular weight is not a decision variable, the M_w spans wide variation at $z = 0$ and $z = L$. Moreover, the warm air temperature optimal profile is not easy to guess by heuristic approaches and features smooth variations.

Notice that the monomer temperatures at the four points shown in Figure 3 have the same shape until 150 min. Up to

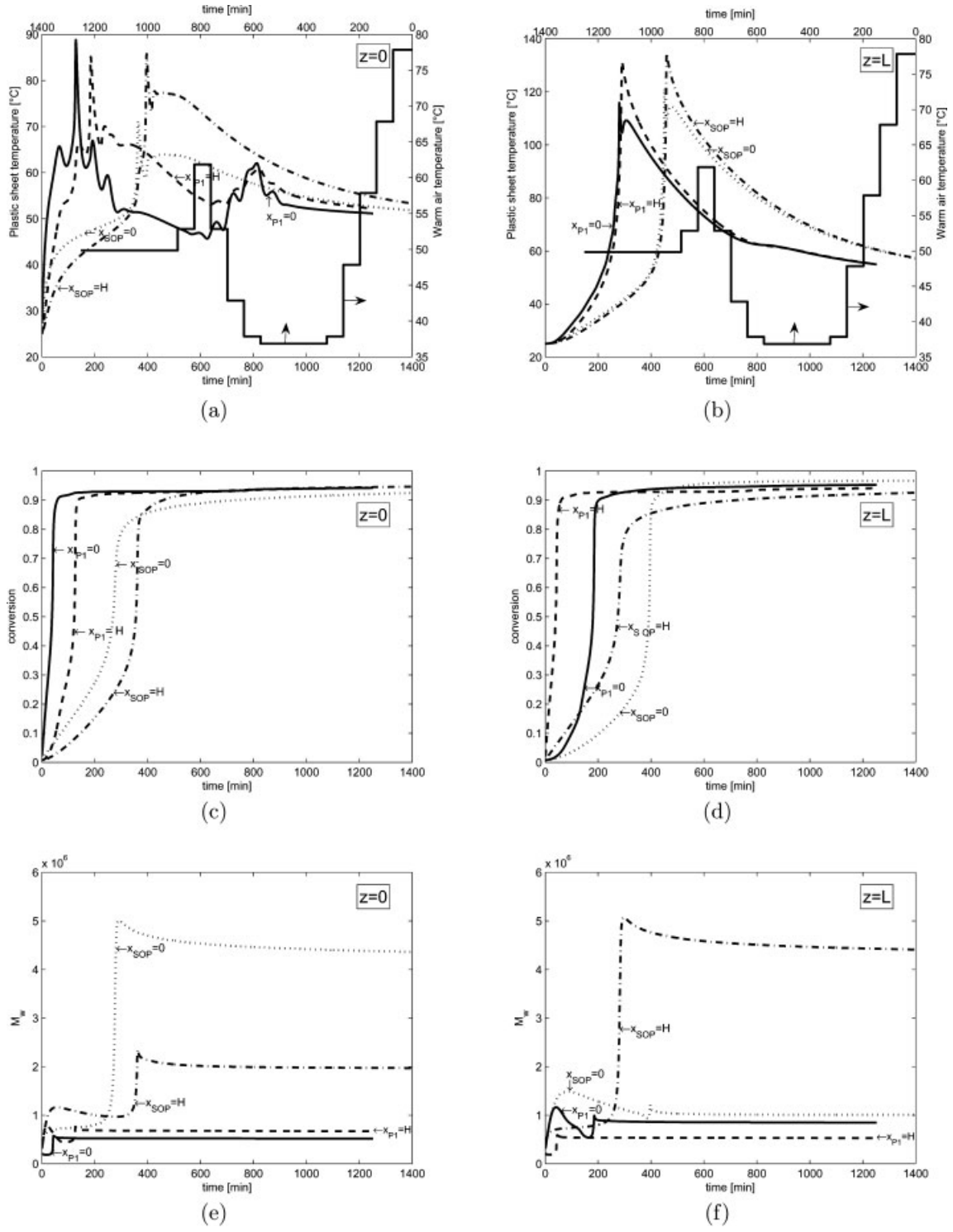

Figure 9. Case 3. Monomer temperature, conversion, and weight average molecular weight dynamic optimal responses and comparison against SOP results for P_1 formulation, 18 mm thickness, and 78°C initial warm air temperature.

The stairs line stands for the warm air optimal profile.

this time the process behaves rather smoothly, i.e., the monomer temperature remains almost constant after the initial peak rise. From 150 to 200 min, the decrease in the propagation rate together with the ongoing propagation phenomenon causes a rapid growth of the free-radical species, hence a higher conversion rate; the movements of polymer chains are restricted as a result of the high viscosity of the reaction mixture. This leads to a dramatic decrease in the termination rate

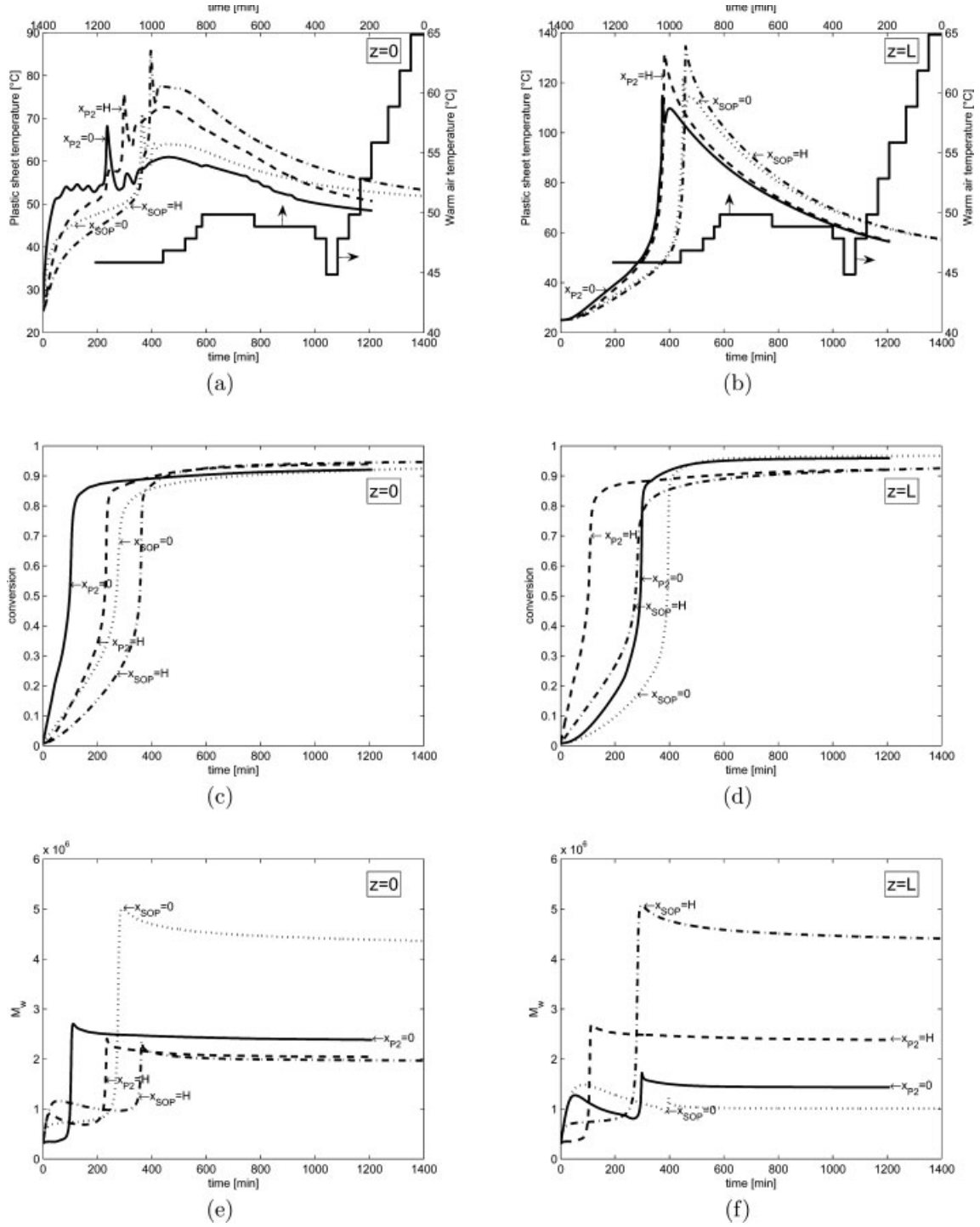

Figure 10. Case 4. Monomer temperature, conversion, and weight average molecular weight dynamic optimal responses and comparison against SOP results for P_2 formulation, 18 mm thickness, and 65°C initial warm air temperature.

The stairs line stands for the warm air optimal profile.

constant and significant auto acceleration of the polymerization because of the increased free radical concentration. Thus, at extremely high conversions, even the movements of small molecules are restricted, lowering the propagation rate constant and possibly leading to a complete termination of the polymerization process. Therefore, the portion of the conversion curve under examination would be concave. A higher amount of heat is released and the polymer reaction temperature also increases, but at this moment, the warming air temperature falls down to remove the heat generated.

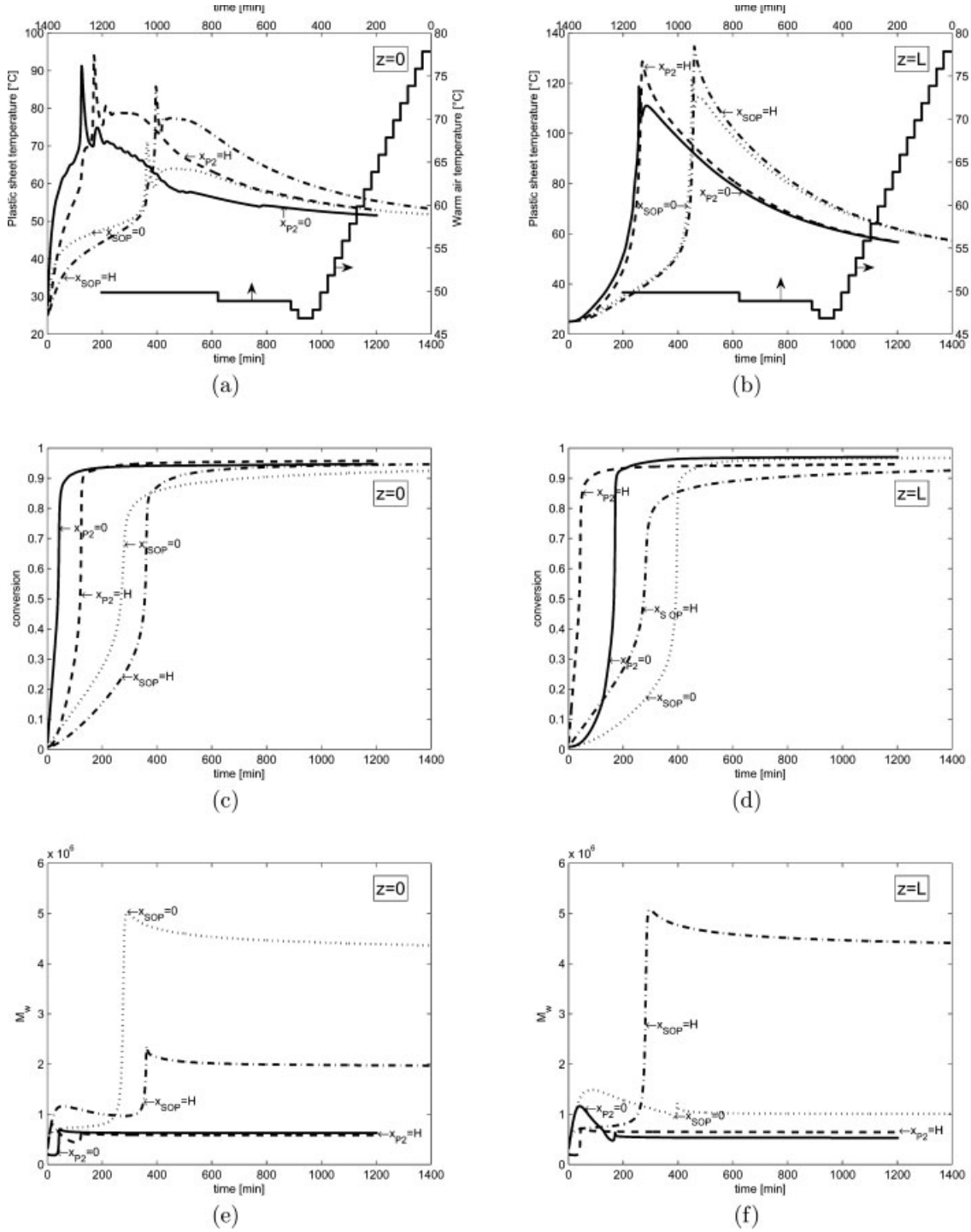

Figure 11. Case 4. Monomer temperature, conversion, and weight average molecular weight dynamic optimal responses and comparison against SOP results for P_2 formulation, 18 mm thickness, and 78°C initial warm air temperature.

The stairs line stands for the warm air optimal profile.

We decided to test the sensitivity of the dynamic optimal results to variations in the initial warm air temperature that was initialized at 70°C. Figure 5 displays the dynamic optimal results and compare them against SOP results. It can be seen that a further reduction in the polymerization time can be achieved by using larger initial warm air temperatures. In fact, at $z = 0$, the plastic sheet temperature has achieved its target value in around 120 min whereas 320 min are required using SOP temperature value. Because of the higher initial air temperature, larger temperature peaks emerge. Moreover, the slope of the classical s-shaped gel effect curve changes rather quickly helping to explain the reduction in polymerization

Table 1. Design Data for Sheet Reactor

Monomer and initiator initial concentration	$M_0 = 9.98$ and $I_0 = 0.0258$	mol/dm^3
Monomer conversion	$X = 0$	
Living and dead moments	$\lambda_i = 0$ and $\mu_i = 0$, $i = 0,1,2$	mol/dm^3
Heat of reaction	$\Delta H = -58.19$	kJ/mol
Polymer density	$\rho = 1200$	kg/m^3
Polymer thermal conductivity	$k = 0.09$	W/(m K)
Polymer heat capacity	$C_p = 1674$	J/(kg K)
Initial air temperature	$T_{a0} = 338.15$ and 351.15	K
Initial monomer temperature	$T_0 = 298.15$	K
Sheet length	$L = 1.8$	m
Sheet thickness	$2H = 0.006$ and 0.018	m
Initiator efficiency	$f = 0.58$	
Target plastic sheet temperature	$T = 50$	C
Target warm air temperature	$T_a = 50$	C
Target weight average molecular weight	$M_w^d = 2.5 \times 10^6$	

times. It is also interesting to note that this time M_w variations are less notorious. In fact, the increase in the polymerization temperature partially suppresses the large increase in M_w because of the gel effect. The M_w final values are lower, up 70%, when compared with Figure 4. Although this time the warm air optimal temperature profile features a step-like shape, the switching times may be difficult to estimate by heuristic or trial and error approaches. The objective function values for the $T_{a0} = 65$ and $T_{a0} = 78$°C cases were 0.0903 and 0.6901 and the optimal warming temperature profiles were computed in around 122 and 166 s CPU time, respectively. These results are summarized in Table 2.

Case 2: P_2, 6 mm, 65 and 78°C

In this case study, we decided to address the benefits of including the M_w as a decision variable. Dynamic optimal results are shown in Figure 6 for a 6 mm thickness when warm air temperature was initialized at 65°C. We note that the optimization results establish a trade-off between monomer conversion and M_w. This time, in comparison with results displayed in Figure 4, the system response is sluggish. However, better control on the M_w (and therefore on mechanical polymer properties) is achieved as shown in Figure 6e, f. This result is, of course, not totally unexpected because the optimization formulation has available more freedom degrees. The proposed dynamic optimization formulation improves those product features that result in homogeneous PMMA properties without significantly increasing the casting time. Moreover, the manipulated variable features smooth changes.

On the other hand, when the warm air temperature is initialized at 78°C, the results shown in Figure 7 are not better (in terms of M_w uniformity) than those obtained without considering the MWD as decision variable (see Figure 5). In fact, the results displayed in Figures 7e, f feature a wide M_w variation compared with similar results shown in Figures 5e, f. The reason for getting poorer MWD homogeneity has to do with the rather small but frequent warm air temperature variations as seen in Figure 7a. Therefore, contrary to what was stated earlier, this time homogenous polymer features can not be improved by simply increasing the warm air initial temperature up to its maximum value subject to operating constraints. As shown in Table 2, both the value of the objective function and CPU time increases because of the additional degree of freedom. However, CPU solution times remain modest.

Case 3: P_1, 18 mm, 65 and 78°C

In this case study, the optimal dynamic results for a 18 mm thickness plastic sheet and warm air initial temperature of 65°C are compared against similar results using SOP. Intuitively, one should expect larger polymerization times because more material and stronger heat transfer limitations are presented. This time, as displayed in Figure 8, the plastic sheet attaints its target value in around 800 min at $z = 0$ and in 1000 min at $z = L$. Figures 8c, d display initially fast polymerization rates, but a rather slow consumption of the remaining monomer. However, the M_w (although no used as a decision variable) stays relatively closed to its target value. On the other hand, if the warm air initial temperature is set at 78°C the polymerization process takes place faster as displayed in Figure 9. This time, the monomer conversion attains large values even at short processing times as shown in Figures 9c and 9(d). However, as seen from Figures 9e, f, achieving faster monomer conversion results in larger M_w deviation from its target value, a situation that should be avoided.

It can be noted from Figures 8a,b that the gel effect remains from 75 to 450 min and that the maximum value of

Table 2. Summary of Results Obtained on a Pentium IV Computer with 2.8 GHz Clock Speed and 512 KB RAM

No.	Case	Thickness (mm)	T_{a0} (°C)	NFE	Objective Function	CPU Time (s)
1	P_1	6	65	20	0.0903	122
2	P_1	6	78	20	0.6901	166
3	P_2	6	65	26	16.958	538
4	P_2	6	78	20	15.992	468
5	P_1	18	65	20	1.0511	240
6	P_1	18	78	20	1.3378	296
7	P_2	18	65	30	18.624	1431
8	P_2	18	78	40	21.175	1874
9	θ_p changed by +5%	6	65	20	0.1663	374
10	θ_p changed by −5%	6	65	20	0.2337	348
11	θ_p changed by +5%	18	65	30	1.3729	585
12	θ_p changed by −5%	18	65	28	1.4650	467

In all the cases $N_x = 5$, $N_z = 8$ and three internal collocation points were used.

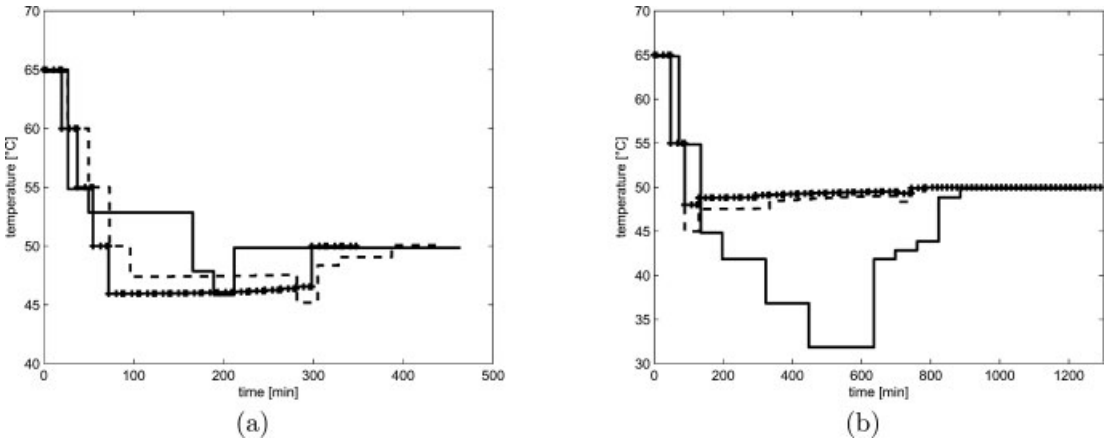

Figure 12. Warm air temperature dynamic optimal sensitivity response using P_1 formulation and 65°C initial air temperature.

The solid line stands for the nominal response, (-+-) is the response for 5% θ_p change whereas (−−) represents the response for −5% θ_p change. (a) 6 mm and (b) 18 mm thickness.

the monomer temperature was much higher compared with the 6 mm thickness plastic sheet because the heat conduction resistance is three times greater. Although the temperature profile shape looks similar, the difference of the maximum peak temperature tends to rise as sheet thickness is increased. Therefore, the internal temperature profiles ($x = 0$) tend to be higher than the external ones ($x = H$). The temperature difference is 10°C at the initial edge ($z = 0$), but at the end edge is 2°C. However, when the gel effect occurs (75 min), we observe 20 and 7°C temperature difference at the same positions when the phenomena have finished. Internal temperature profiles are larger than the external ones because of the cooling effect of air flowing over the plastic sheet. Moreover, as the polymerization reaction goes on, polymer viscosity increases leading to conduction heat transfer limitations. Hence, heat dissipation becomes harder to achieve. Because the initial edge ($z = 0$) of the sheet reactor is closer to the heat source (the warming air flow rate), the temperature rise in this zone is higher than in the opposite side of the sheet ($z = L$). This the reason why the gel effect occurs first there rather than in the opposite side of the system. Because the initial edge of the sheet is the one with the fastest temperature response, it is also the one with the highest amount of instantaneous heat release because of the exothermic nature of the MMA polymerization reaction; this phenomenon clearly contributes to an even higher temperature rise. Even though the presence of this sudden temperature rise, due to the onset of the auto acceleration effect, the heat transfer resistance in the internal part of the sheet is higher than the one presented by the glass at its external surface. Hence, most of the heat flow is exchanged at the interface by convection with the flowing air. At the internal point, 100 and 425 min are required to achieve 80% monomer conversion ($x = 0$), whereas at the external point, 380 and 100 min were required ($x = H$) for optimal operation. The plastic sheet thermal behavior affects the monomer conversion and the molecular weight distribution. The inner temperature is greater than the surface temperature. When the air temperature decreased from 65 to 32°C, the heat produced by the reaction is removed by the air. From 450 min on, where the temperatures for the initial edge of the sheet are smaller than the desired temperature (50°C), the air temperature increase gradually on six steps from 32 to 50°C to consume the remaining monomer. Even with the increase in plastic sheet thickness, the CPU solution time remain low as shown in Table 2.

Case 4: P_2, 18 mm, 65 and 78°C

In this final case study, the effect of using the M_w as decision variable and different warm air initial temperatures was addressed for a 18 mm thickness plastic sheet. As seen from Figure 10, improved M_w uniformity was achieved by using warm air initially heated up to 65°C. As expected, M_w homogeneity is best achieved at $z = 0$ (see Figure 10e). At $z = L$, M_w uniformity is acceptable specially at the plastic sheet surface (see Figure 10f). Again, it should be noted that the polymerization rate (measured in terms of monomer conversion) is not as fast as it was observed in past cases (i.e., neglecting M_w as decision variable). However, if the polymerization process takes place at a slower rate better polymer homogeneity features can be obtained. On the other hand, as displayed in Figure 11, if the warm air initial temperature is increased up to 78°C the polymerization rate takes place faster (see Figures 11c, d), but polymer homogeneity is difficult to enforce as shown in Figures 11e, f. The results obtained up to now indicate that homogenous polymer properties might be easier to achieve using M_w as decision variable.

It can be observed that thicker sheets increases the overall batch operation time from 400 min for 6 mm to 1200 min for 18 mm thickness, but results in smaller deviations of the quality variables from their respective desired final values. The forced-circulation warm air oven provides the best protection against overheating the sheet, develops the least amount of temperature gradient throughout the sheet, results in shorter warming and polymerization operational times, and is recommended when manufacturing plastic sheets of large thickness. Different heating times and warming air temperature profiles were obtained depending on the form of the objective function and the thickness of plastic sheet. As

shown in Table 2 including M_w as additional degree of freedom leads to a five times increase in the CPU solution time.

Case 5: Varying kinetic parameters

Although polymerization of MMA is one of the most widely studied polymerization systems, there remains considerable uncertainty in the true kinetic model, especially in the characteristic monomer diffusion time for propagation, θ_p, and termination, θ_t steps whose nominal values may change during reactor operation. These parameters are embedded in the rate constants of propagation, k_p, and termination, k_t, steps, respectively. The overall chain termination rate constant, k_t, is the sum of combination and disproportionation contributions, $k_t = k_{tc} + k_{td}$, with each one assumed to feature Arrhenius temperature dependence, see Eqs. 7a–l. Uncertainties in the propagation rate constant are important, not only because this step is proportional to the rate of polymer conversion but because it strongly affects the molecular weight distribution. In this regard, even when in this work the effects of uncertainty were not fully addressed, a parameter sensitivity analysis was carried out. The sensitivity of the dynamic optimal model response was sought for small changes on θ_p by $\pm$ 5% as shown in Figures 12–14.

The warm air optimal temperature profile features stronger dependence when θ_p is underestimated as displayed in Figure 12. As the thickness of the plastic sheet increases so does the sensitivity of the optimal temperature profile as shown in Figure 12b. This observation is corroborated on the PMMA polymerization reactor response displayed in Figures 13 and

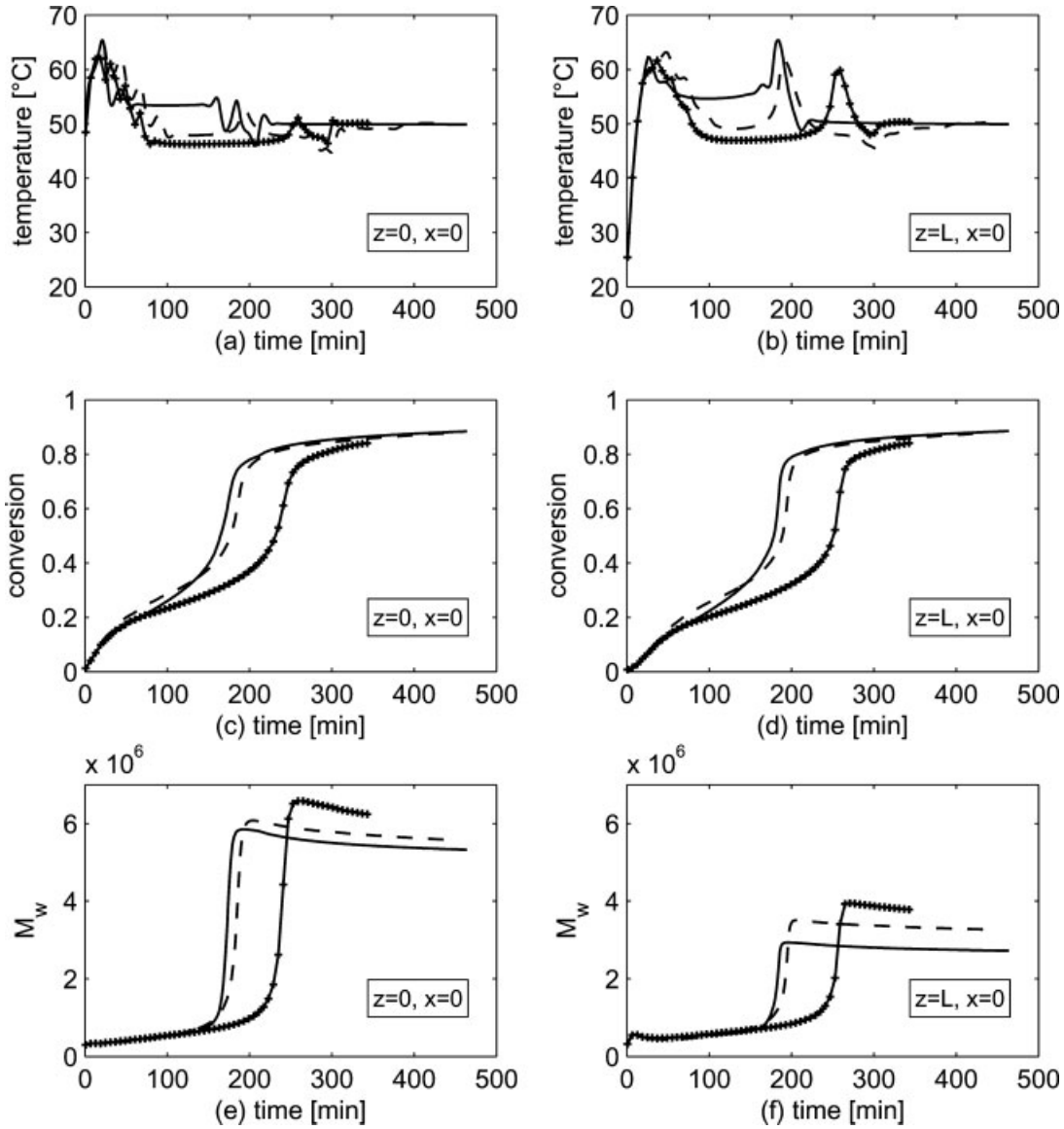

Figure 13. Monomer temperature, conversion, and weight average molecular weight dynamic optimal sensitivity response using P_1 formulation, 6 mm thickness, and 65°C initial air temperature.

The solid line stands for the nominal response, (-+-) is the response for 5% θ_p change whereas (−−) represents the response for −5% θ_p change.

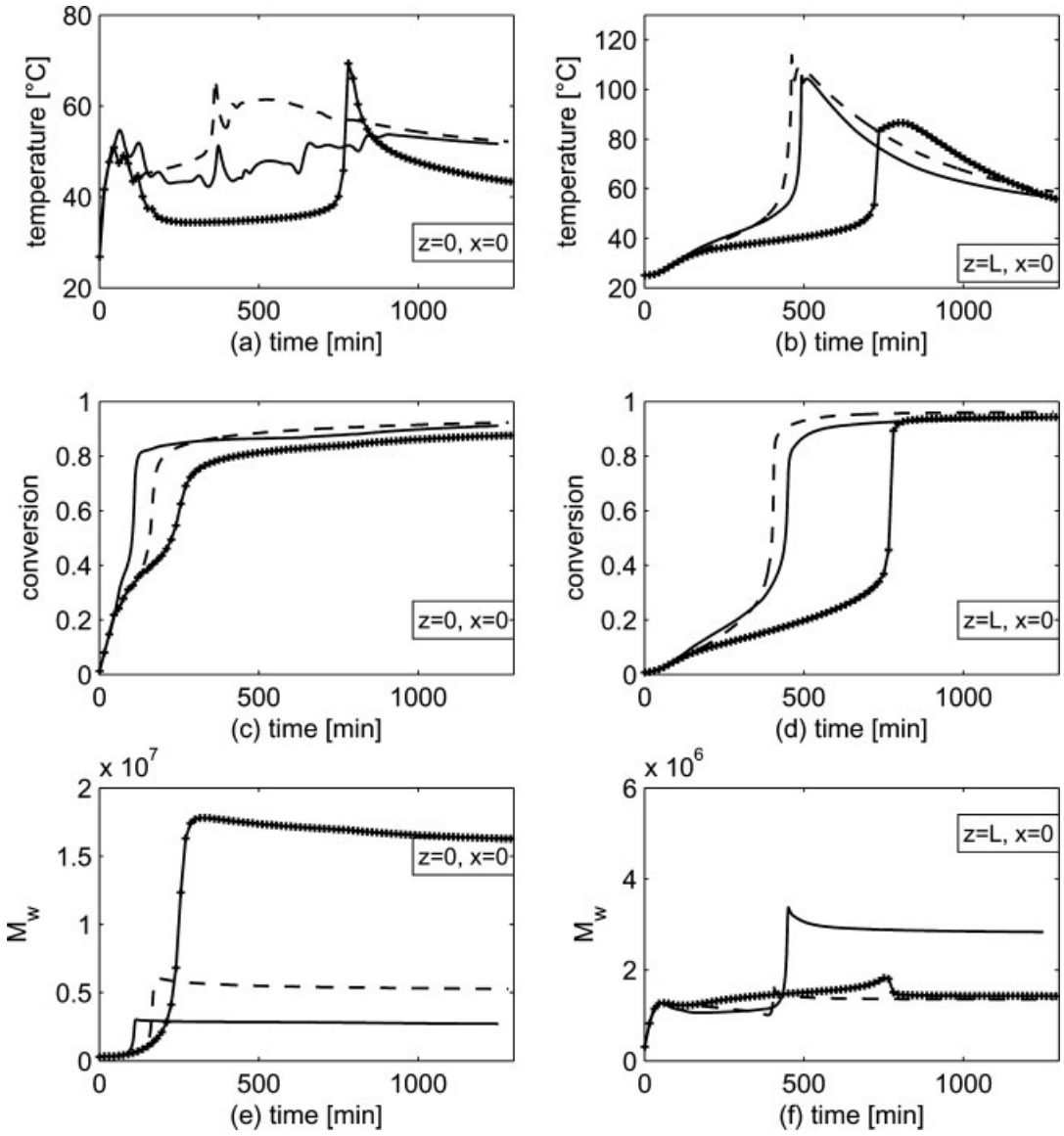

Figure 14. Monomer temperature, conversion, and weight average molecular weight dynamic optimal sensitivity response using P_1 formulation, 18 mm thickness, and 65°C initial air temperature.

The solid line stands for the nominal response, (-+-) is the response for 5% θ_p change whereas (−−) represents the response for −5% θ_p change.

14 for 6 and 18 mm thickness, respectively. In these Figures, the greatest system sensitivity to θ_p variations (mainly when θ_p was underestimated) was observed for the thicker plastic sheet, especially for the M_w dynamic optimal response (see Figures 14e, f). In comparison as the thickness of the plastic sheet diminishes so does the dependence of the optimal response to θ_p variations. This behavior can be appreciated in Figures 13e, f where M_w displays a smooth dependence on θ_p. It should be remarked that the sensitivity of the system optimal response was also addressed in face of θ_t variations. However, in this case, the system sensitivity featured smaller dependence compared with θ_p changes. Although this results seems appropriate behavior of the diffusion controlled model, there are several models published dealing with the mathematical description of diffusion-controlled kinetic rate constants in free-radical polymerization. These have been reviewed by O'Neil and Torkelson,[24] Dube et al.,[14] Nising and Meyer.[25] In all the models, the expressions for termination rate coefficient, k_t, and propagation coefficient rate k_p are composed of a chemical reaction term and a physical diffusion term. Some authors, for instance Vivaldo-Lima et al.,[15] give detailed guidelines for the evaluation of diffusion controlled models to compare its predictive ability for results interpolation and extrapolation purposes.

Conclusions

This work presented a formulation for the dynamic optimization of the MMA cell-cast process for plastic sheet production taking place in a force-circulated warm air reactor.

The proposed optimization formulation allows a flexible implementation of the process operation limits, monomer temperatures constraints (e.g., risk of bubble formation) as well as different objective functions, which give rise to the different polymerization scenarios.

On one hand, when using the P_1 formulation the results indicate that good monomer conversion (measured in terms of polymerization processing time) can be attained by operating at high initial warm air temperatures. However, improving conversion tends to produce plastic sheets featuring poor M_w control. On the other hand, better results were obtained by using the P_2 optimization formulation where M_w became a decision variable. The results clearly indicate that there is a trade-off between monomer conversion and M_w. In this case, one of the best optimal solutions state that allowing sluggish monomer conversion response helps to improve the control on the M_w. Of course, this trade-off is a consequence of using monofunctional initiators. In future work, we will explore the advantages of using bi- and tri-funcional initiators to simultaneously improve both polymerization rate and M_w.

In all the addressed case studies, the dynamic optimal operation of the force-circulated warm air reactor demanded less polymerization processing time when compared against isothermal operating policies. Even when an economical analysis was not done, this result is an indication that the optimization results should increase process profit because smaller amounts of auxiliary services would be required.

The results also indicate that to get smaller processing times, the force-circulated warm air reactor should be started at an initial air temperature larger than the target monomer temperature. We ran some case studies starting the reactor at an initial air temperature close to environment conditions (20°C) and, as expected, the optimal results featured larger processing times.

Even when only local optimal solutions were sought, we think that the reported solutions are some of the best ones we might determine, especially for the P_1 formulation because it features small objective function values. Although the objective function values of the P_2 formulation feature large values, we obtained the same solutions starting from different initial guesses of the decision variables. Although when the thermal and kinetic effects of the addressed systems are complex, the computational load for finding optimal solutions was relatively modest. Therefore, real time control of the addressed polymerization system seems to be feasible and it will be addressed in a future work.

Acknowledgements

This work was supported by Universidad Iberoamericana.

Notation

a = thickness-to-length ratio for plastic sheet (dimensionless)
A_k = coefficients for dimensionless Eqs. 4–6, k = 1, 2, 3, 4 (dimensionless)
A_{km} = matrix element for orthogonal collocation method
B_i = biot number in any coordinate, x or z (dimensionless)
C_p = heat capacity [J/(kg K)]
f = initiator efficiency
h = heat transfer coefficient [$W/(m^2$ K)]
H = sheet thickness (m)
I = molar concentration of initiator (mol/dm^3)
$\bar{I}$ = dimensionless molar concentration of initiator
k = thermal conductivity [$W/(m$ K)]
k_d = kinetic coefficient for initiator (1/min)
$\bar{k}_d$ = dimensionless kinetic coefficient for initiator
k_i = kinetic coefficient for initiation reaction [dm^3/(min mol)]
k_p = kinetic coefficient for propagation [dm^3/(min mol)]
$\bar{k}_p$ = dimensionless kinetic coefficient for propagation
k_f = kinetic coefficient for chain transfer to monomer [dm^3/(min mol)]
$\bar{k}_f$ = dimensionless kinetic coefficient for chain transfer to monomer
k_{tc} = kinetic coefficient for termination by addition [dm^3/(min mol)]
$\bar{k}_{tc}$ = dimensionless kinetic coefficient for termination by addition
k_{td} = kinetic coefficient for termination disproportionation [dm^3/(min mol)]
$\bar{k}_{td}$ = kinetic coefficient for termination disproportionation
L = sheet length (m)
M = molar concentration of monomer (mol/dm^3)
M_n = number-average molecular weight (kg/kmol)
M_w = weight-average molecular weight (kg/kmol)
M_w^m = monomer molecular weight (kg/kmol)
N_c = number of collocation points (dimensionless)
N_e = number of finite elements (dimensionless)
N_x = number of points for discretization on x-direction (dimensionless)
N_z = number of points for discretization on y-direction (dimensionless)
P_r = Prandtl number (dimensionless)
Q = heat released by the polymerization reactions (W/m^3)
$\bar{Q}$ = dimensionless heat released by the polymerization reactions
R = universal gas constant [kJ/(mol K)]
R_e = Reynolds number dimensionless
T = polymer temperature (K)
T_a = air temperature (K)
T_g = glass transition temperature of the pure polymer (K)
T_0 = initial monomer temperature (K)
t = reaction time (min)
W = sheet width
X = monomer conversion
$\bar{Y}$ = dimensionless Y state
$\dot{Y}$ = first order derivative of the Y state
x = x-axis for the sheet thickness (m)
z = z-axis for the sheet length (m)

Greek letters

α = thermal diffusivity (m^2/min)
ΔH_r = heat of polymer reaction (kJ/mol)
θ = dimensionless temperature
θ_a = dimensionless air temperature
θ_g = dimensionless glass transition temperature
Θ_p = monomer diffusion time for propagation stage
Θ_t = monomer diffusion time for termination stage
ε = volume expansion factor (dimensionless)
λ_0 = zeroth moment of the growing radicals (mol/dm^3)
$\bar{\lambda}_0$ = dimensionless zeroth moment of the growing radicals
λ_1 = first moment of the growing radicals (mol/dm^3)
$\bar{\lambda}_1$ = dimensionless first moment of the growing radicals
λ_2 = second moment of the growing radicals (mol/dm^3)
$\bar{\lambda}_2$ = dimensionless second moment of the growing radicals
μ_0 = zeroth moment for the dead polymer (mol/dm^3)
$\bar{\mu}_0$ = dimensionless zeroth moment for the dead polymer
μ_1 = first moments for the dead polymer (mol/dm^3)
$\bar{\mu}_1$ = dimensionless first moment for the dead polymer
μ_2 = second moments for the dead polymer (mol/dm^3)
$\bar{\mu}_2$ = dimensionless second moment for the dead polymer
ν = kinematic viscosity (m^2/min)
ρ = density (kg/m^3)
τ = dimensionless operating time
ξ = dimensionless variable for x coordinate
ζ = dimensionless variable for z coordinate

Subscripts

a = air
i = position in x-direction
j = position in z-direction
k, n = number of collocation point
m = number of finite element
tr = transition time
rxn = reaction

Superscripts

d = desired value
0 = starting value

Literature Cited

1. Kiparissides C. Polymerization reaction modeling: a review of recent developments and future directions. *Chem Eng Sci.* 1996;51:1637–1659.
2. Kameswaran S, Biegler LT. Simultaneous dynamic optimization strategies: recent advances and challenges. *Comput Chem Eng.* 2006;30:1560–1575.
3. Biegler LT, Ghattas O, Heinkenschloss M, van Bloemen Waanders B. *Large-scale PDE-Constrained Optimization*. Berlin: Springer, 2003.
4. Allgor RJ, Barton P. Mixed-integer dynamic optimization. I. Problem formulation. *Comput Chem Eng.* 1999;23:567–584.
5. Biegler LT, Saldívar-Guerra E, Flores-Tlacuahuac A. Optimization of HIPS open-loop unstable polymerization reactors. *Ind Eng Chem Res.* 2005;44:2659–2674.
6. Flores-Tlacuahuac A, Rivera-Toledo M, García-Crispín LE, Vílchis-Ramírez L. Dynamic modeling and experimental validation of the mma cells cast process for plastic sheet production. *Ind Eng Chem Res.* 2006;45:8539–8553.
7. Soong DS, Louie BM. Optimization of batch polymerization processes— narrowing the mwd. I. Model simulation. *J Appl Polym Sci.* 1985;380:3707–3749.
8. Soroush M, Kravaris C. Optimal design and operation of batch reactors. II. A case study. *Ind Eng Chem Res.* 1993;32:882–893.
9. Wachter A, Biegler LT. *Algorithm for Large-Scale Nonlinear Programming*. Technical report, CAPD Technical Report B-00-06, Carnegie-Mellon Univesity, 2000.
10. Gay DM, Fourer R, Kernighan BW. *AMPL A Modeling Language for Mathematical Programming*, 2nd ed. Thomson, Brooks/Cole, 2003.
11. Rosetti C. *Apparatus for Casting Plastic Sheet*. U.S. Patent 3,689,022, 1973.
12. Daddona P. *Apparatus for the Production of Case Polymer Sheets*. U.S. Patent 3,694,129, 1972.
13. Odian G. *Principles of Polymerization*. Wiley Interscience, 1991.
14. Dubée MA, Soares JBP, Penlidis A, Hamielec AE. Mathematical modeling of multicomponent chain-growth polymerizations in batch, semibatch, and continuous reactors: a review. *Ind Eng Chem Res.* 1997;36:966–1015.
15. Vivaldo-Lima A, Hamielec AE, Wood PE. Auto-acceleration effect in free radical polymerization. A comparison of the CCS and MH models. *Polym React Eng.* 1994;2:17–85.
16. Mourikas G, Kiparissides C, Seferlis P, Morris AJ. Online optimizing control of molecular weight properties in batch free-radical polymerization reactors. *Ind Eng Chem Res.* 2002;41:6120–6131.
17. Achilias DS, Kiparissides C. Development of a general mathematical framework for modeling diffusion-controlled free radical polymerization reactions. *Macromolecules.* 1992;25:3739–3750.
18. Bird RB, Stewart WE, Lighfoot EN. *Transport Phenomena*. John Wiley, 2001.
19. Chiu WY, Carrat GM, Soong S. A computer method for the gel effect in free radical polymerization. *Macromolecules* 1983;16:348–357.
20. Stewart MD. *Catalyst Diffusion in Positive-Tone Chemically Amplified Photoresists*. PhD Thesis, The university of Texas at Austin, 2003.
21. Nunes RW, Martin JR, Johnson JF. Influence of molecular weight and molecular weight distribution on mechanical properties of polymers. *J Polym Sci A: Polym Chem.* 1982;22:205–228.
22. Takamatsu T, Shioya S, Okada Y. Molecular weight distribution control in a batch polymerization. *Ind Eng Chem Res.* 1988;27:93–99.
23. Schiesser WE. *The Numerical Method of Lines. Integration of Partial Differential Equations*. Academic Press, Inc., 1991.
24. O'Neil GA, Torkelson JM. Recent advances in the understanding of the gel effect in free radical polymerization. *Trends Polym Sci.* 1997;5:349–355.
25. Nising P, Meyer T. Modeling of the high-temperature polymerization of methyl methacrylate. I. Review of existing models for the description of the gel effect. *Ind Eng Chem Res.* 2004;43:7220–7226.

Manuscript received Dec. 21, 2007, and revision received Dec. 1, 2008.